Modulation of DNA Loop Lifetimes by the Free Energy of Loop Formation: Supplementary Information

Yi-Ju Chen[1,†], Stephanie Johnson[2,3,†], Peter Mulligan[4,†], Andrew Spakowitz[4], & Rob Phillips[5,*]

October 8, 2014

1 Department of Physics, California Institute of Technology, Pasadena, CA, USA

2 Department of Biochemistry and Molecular Biophysics, California Institute of Technology, Pasadena, CA, USA

3 Present address: Department of Biochemistry and Biophysics, University of California San Francisco, San Francisco, CA, USA

4 Department of Chemical Engineering, Stanford University, Stanford, CA, USA

5 Departments of Applied Physics and Biology, California Institute of Technology, Pasadena, CA, USA

∗ E-mail: phillips@pboc.caltech.edu

† These authors contributed equally to this work.

Contents

List of Figures

List of Tables

S1 Supplementary Methods: Data Analysis

S1.1 Data acquisition and analysis overview.

In this work, we use the conventional half-amplitude thresholding method, described in the next section, to quantify looped and unlooped state durations ("lifetimes," also referred to in the literature as dwell times) in the tethered particle motion (TPM) data of (1, 2). These data were obtained with Lac repressor purified in-house and used at a final concentration of 100 pM except as indicated in Fig. S3 below. DNA constructs consisted of loop lengths ranging from roughly 90 to 120 bp, composed of the five sequences described in Fig. S1a: The synthetic, random E8 sequence (3, 4), the synthetic, strong nucleosome positioning sequence 601TA which we abbreviate "TA" (3–5), the strong naturally occurring 5S nucleosome positioning sequence (6), a poly(dA:dT)-rich DNA from a nucleosome-free region of a yeast promotor that we call "dA" (7), and a CG-rich sequence from humans that we call "CG" (8). The loop sequence is flanked by various combinations of operators that are known to have different affinities for the Lac repressor: O_{id}, the strongest, O_1, roughly 4 times weaker, or O_2, about 5 times weaker than O_1. The affinities of the Lac repressor for these operators as measured by TPM are within those measured by traditional ensemble biochemical assays, as described in our previous work (1, 2). In the main text we focus on the very strong, synthetic O_{id} operator and the weaker naturally occurring O_1 operator; data with additional operators are discussed briefly below. Roughly 150 bp of DNA separated the operators and the bead or the microscope slide, for total tether lengths of around 450 bp. Details of these constructs can be found in Fig. S1a and in Refs. (1, 2); in figure legends constructs are referred to as <operator><loop sequence and length><operator>.

To summarize our previous work with these constructs, a DNA's sequence and length affect its bending and torsional rigidities and its helical repeat, which in turn affects the relative phasing of the two operators, and, it has been proposed, the conformation of the repressor protein in the looped state (9–14). Thus by fine-tuning DNA sequence and loop length systematically, we were able to generate a library of looping J-factors (J_{loop}) for this work. (For comparison with our theoretical framework, we focus here on simply the total looped state lifetimes, although we discuss briefly below subtleties arising from possible additional repressor conformations and/or loop structures.)

Details of our implementation of the half-amplitude thresholding procedure used to quantify looped and unlooped lifetimes are given in the next section. For each data point in the figures in this work (that is, data for a particular DNA construct at a particular repressor concentration), we obtain distributions of looped and unlooped lifetimes from roughly 30-50 tethers, observed from 10 to 100 minutes. Examples of these distributions are given in Sec. S3.1 below. We report the means of these distributions and the standard errors on the means. A comparison of our results to those in previous studies using TPM to measure Lac repressor looping and unlooping rates, showing good agreement between our results and these previous studies, is given in Sec. S3.2.

S1.2 Kinetic analysis by half-amplitude thresholding.

In this work we used the conventional half-amplitude thresholding method (13, 17, 19–23) to obtain kinetic parameters from TPM data. An outline of this method is shown in Fig. S1. The basic concept of this method is to define thresholds, or root-mean-squared (RMS) values of the bead's motion, that delineate different states (for example, that define the difference between "unlooped" and "looped"), and then to define the lifetime of a particular state as the time during which a bead's RMS does not cross a threshold. The subtleties in this method arise from dealing with spurious events (for example, short-lived sticking events), and the limited time resolution of the Gaussian filter that is applied to the RMS trace before the lifetime analysis is done (see details in (1)). Our treatment of these subtleties is described below.

Trajectories were thresholded as described in (1), using the minima between Gaussians fit to the RMS histogram to define preliminary thresholds, which were manually adjusted as needed. The result of this

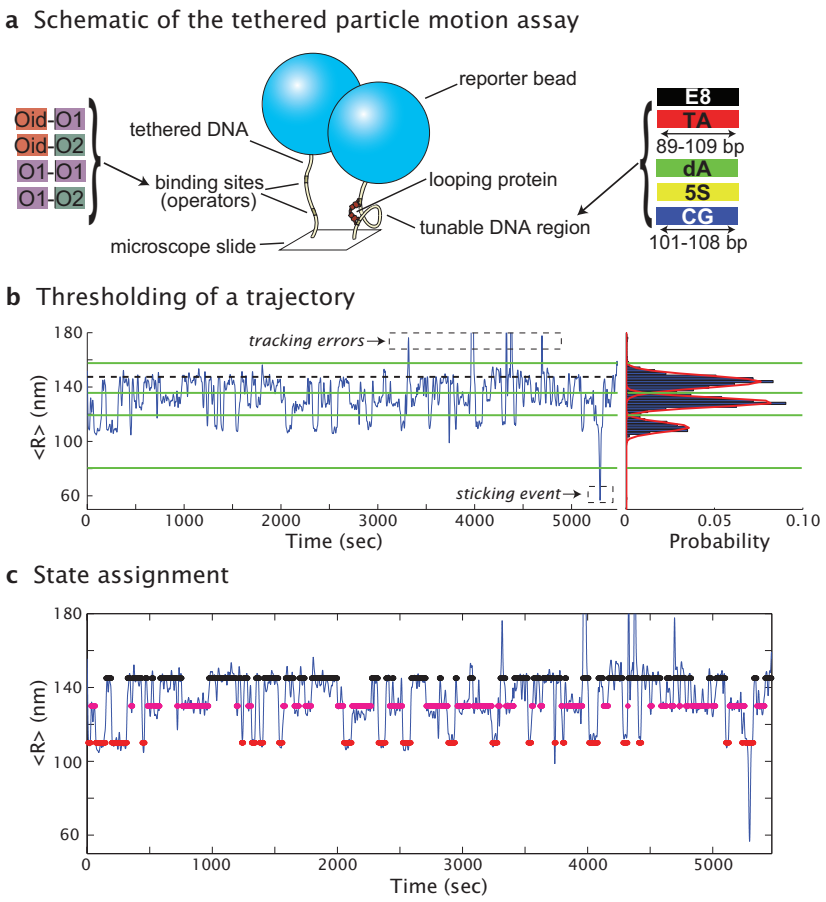

Figure S1: **Half-amplitude thresholding for obtaining kinetic information from TPM traces. a,** In tethered particle motion, single DNA molecules tether microscopic beads to the surface of a slide. The formation of a loop between two Lac repressor binding sites (operators) by the Lac repressor protein causes the motion of the bead to be reduced. By calculating the time-averaged root-mean-squared ("$\langle R \rangle$") motion of the bead over time, we can detect looping and unlooping events (1, 15–18) (more precisely, $\langle R \rangle$ is our shorthand for the Gaussian-filtered root-mean-squared motion [sqrt($x_t^2 + y_t^2$)] of the bead, where x_t and y_t are a bead's (x, y) position at time t). The constructs used in this work contain varying lengths of DNA in the tunable DNA region, composed of five different sequences (the synthetic, random E8 sequence (3, 4), the synthetic, strong nucleosome positioning sequence 601TA which we abbreviate "TA" (3–5), the strong naturally occurring 5S nucleosome positioning sequence (6), a poly(dA:dT)-rich DNA from a nucleosome-free region of a yeast promotor that we call "dA" (7), and a CG-rich sequence from humans that we call "CG" (8)), and flanked by various combinations of operators that are known to have different affinities for the Lac repressor: O_{id}, the strongest, O_1, roughly 4 times weaker, or O_2, about 5 times weaker than O_1 (1, 2). **b,** A sample TPM trajectory from a single bead, one that exhibits three genuine states (unlooped plus "middle" and "bottom" looped states) and several spurious states (both tracking errors and sticking events). The righthand panel shows a histogram of the $\langle R \rangle$ values for this trajectory. Red lines indicate a fit of three Gaussians to the histogram; thresholds (green lines) are chosen as the minima between Gaussians, except for the bottommost line, which is set at 80 nm for all traces (the shortest $\langle R \rangle$ that we can distinguish from sticking events), and the topmost line, which is set to the sum of the mean $\langle R \rangle$ in the absence of repressor (black dashed line) plus three standard deviations of the Gaussian fit to the $\langle R \rangle$ histogram in the absence of repressor. **c,** As described in the text, the thresholds defined as shown in (a) are used to assign a state (unlooped, black; middle loop, magenta; or bottom loop, red) to each point in the trajectory. Time spent in spurious states is reassigned to genuine states as described in the text. Note that this figure describes the analysis for calculating middle and bottom looped states separately; for the analyses used in the main text, trajectories were thresholded into unlooped, looped and spurious only.

thresholding allowed every time point in an RMS trace to be assigned a state: "U", unlooped; "M", middle looped state; "B", bottom looped state; or "Sp", spurious. Time points were labeled spurious where the RMS value exceeded the highest threshold (and was therefore most likely due to a tracking error, for example if a free bead in solution passed through the field of view), or where it fell beneath the bottom threshold (and was therefore most likely due to a sticking event). The "bottom" and "middle" looped states refer to the two different looped states, defined as two distinct tether lengths (differing in RMS by about 10 nm), that we and others have observed in looping studies with the Lac repressor (1, 2, 10, 13, 24–29). However, for most of the constructs studied here the occurrence of the bottom state was too infrequent to allow reliable estimates of its mean lifetime. For this reason, and for consistency with the model derived in the main text, the lifetimes shown in the figures in the main text are derived from an analysis in which the threshold between the middle and bottom looped states was ignored, such that trajectories were divided into only unlooped or looped states (and spurious states). Results for the middle state stemming from an analysis in which the bottom and middle looped states were separated out are given in Sec. S3.3 below.

Following the convention in the field (13, 17, 19, 20), we ignored any dwells shorter than twice the dead time of the filter (defined in the next section), treating them as follows: if a transition occurred to a state whose duration lasted shorter than twice the filter dead time, and the states just before and just after this too-short dwell were the same, we counted the flanking dwells plus the time in the too-short dwell as one long lifetime in the flanking state. If the states before and after the too-short dwell were different, however, we split the too-short dwell between the preceding and succeeding dwells. Excluding too-short dwells was performed before the removal of spurious states (so too-short spurious states, as well as too-short genuine states, were ignored).

We dealt with spurious states in a similar manner to too-short dwells: if a spurious state was preceded and followed by the same genuine state, then we assumed the underlying genuine state of the system did not change during the spurious event and considered the flanking dwells plus the time spent in the spurious state to be one long lifetime. If the flanking states were not the same, however, we counted half the spurious event's duration towards the preceding event, and half towards the succeeding event. This approach is reasonable as long as most dwells in spurious states are significantly shorter than the average transition rate between genuine states. For example, if a sticking event occurs that lasts several minutes, and it is preceded and followed by dwells in the unlooped state, but in the rest of the trajectory the unlooped state transitions back and forth to a looped state(s) every few seconds, then it is unreasonable to assume that no transitions occurred during the minutes-long sticking event. We find the mean lifetime of spurious events in our assay to be 30 ± 3 seconds, independent of repressor concentration, loop sequence, loop length, and flanking operators. As can be seen in Fig. S3 and Figs. S9 and S10 below, although the mean lifetimes of genuine states for some constructs approach 30 seconds, the majority are longer. Therefore we consider our treatment of spurious events to be reasonable.[1]

The result of this thresholding procedure is a series of states and times spent in these states, for each trajectory in a data set. The mean and standard error of the lifetimes for a particular state were calculated over all trajectories in a data set. We note here one final subtlety to the calculation of these mean lifetimes, which is whether or not to include the first and last dwells in a given trajectory, whose observed duration is bounded not by transitions to new states, but on one side by the limitation of the

[1] We explored two additional approaches to dealing with spurious events that derive from an alternate assumption, that because we have no information about the true state of the system during a spurious event, we should excise the time spent in spurious states. Then the preceding and succeeding dwells can either be concatenated, as if the spurious event never occurred; or they can be counted as separate, regardless of whether they were the same or different states. Because most spurious states are relatively short-lived, the first approach, that of concatenating trajectories around excised spurious events, yields mean lifetimes that are comparable to those calculated by our chosen approach described above. However, the second approach, that of counting dwells before and after spurious events as entirely separate, leads to calculated lifetimes that are on average about half as long as those calculated from the other methods, because of the introduction of what we believe to be false transitions when no such transition actually occurred. We conclude that the method we followed gave the most reasonable estimate of the true lifetimes in genuine states.

observation time. If the dwells in each genuine state were exponentially distributed, then because of the property of memorylessness of single exponentials, we could include these first and last dwells. However, as noted below in Section S3.1, we find that almost none of the lifetime distributions are exponential. Therefore we excluded the first and last dwell of every trajectory from our analysis. In practice, most data sets contain so many dwells that the inclusion of these two extra dwells per trace did not change the mean lifetimes we calculated, with the exception of data sets for which the looping probability is either very high or very low, where our ability to obtain meaningful information about average lifetimes in the unlooped state (if looping is rare) or the looped state (if the looping probability is very close to 1, for example for the Oid-TA94-O1 construct at most repressor concentrations) is limited regardless of how we treat first and last dwells.

As an additional test of our algorithm for calculating lifetimes, we compared the mean lifetimes that we obtained for the Oid-E8107-O1 construct, at all five repressor concentrations, with mean lifetimes computed using a variational Bayes/hidden Markov model (vb-HMM) approach (30) similar to a method previously described for FRET (31) and single-particle tracking (32). This vb-HMM approach is entirely orthogonal to the thresholding method described here, making use of maximum likelihood estimates of the true state at every point in a trajectory, yet results in comparable mean lifetimes to those shown in Figs. S3a and S3b below. We conclude that, while the vb-HMM approach is preferable for constructs with fast transitions and/or closely spaced states, or, as we argue in (30), for demonstrating that the looped states we observe are composed of multiple microstates, for our purposes here the half-amplitude approach sufficed.

S1.3 Calculating the dead time of a filter.

The "dead time" of a filter refers to the duration of an event (looping or unlooping) that gives a half-amplitude response from the filter (33, 34). The convention in the field is then to assume that the temporal resolution is twice the dead time (13, 17, 19, 20), that is, events shorter than twice the dead time cannot be resolved as true transitions between states instead of noise. In this section we will derive an expression for that dead time for the Gaussian filters that were discussed above.[2]

In this derivation we will consider the true signal from TPM to be a step function, and neglect the noise that is superimposed on this signal (though that noise also contributes to the temporal resolution of the experiment, it is ignored when calculating the filter dead time). For simplicity consider a two-state system, and let state 1 be at RMS = 0, and state 2 at RMS = A. For an event from state 1 to state 2 back to state 1, where the dwell in state 2 lasts time T and is centered at $t = 0$, we can write the corresponding raw, unfiltered TPM trace as

$$x(t) = A \cdot s_T(t), \tag{S1}$$

where $s_T(t)$ is 1 between $t = -T/2$ and $t = +T/2$, and zero elsewhere. Then, by the definition above, the dead time of the filter will be an event duration T that produces a half-amplitude response in the filtered signal, *i.e.* such that the amplitude of the filtered signal becomes $A/2$, when the amplitude of the unfiltered signal is A.

If we apply a Gaussian filter $g(t)$ with some standard deviation σ_g to the step-function "trace", the sharp transitions from states 1 to 2 at $t = -T/2$ and from state 2 to 1 at $t = T/2$ will be smoothed, with the maximum of the filtered signal at $t = 0$, when the filter and underlying trace are aligned. Mathematically, we define "applying a filter" as convolving the filter $g(t)$ with the signal $x(t)$, such that the filtered signal filt_$x(t)$ can be written as

$$\text{filt\_}x(t) = \int_{-\infty}^{+\infty} g(t-\tau)x(\tau)d\tau. \tag{S2}$$

[2]Thanks to Matthew Johnson at MIT for the outline of this derivation.

Because a Gaussian is an even function, that is, symmetric about $t = 0$ such that $g(t) = g(-t)$, we know that at time $t = 0$,

$$\text{filt\_}x(0) = \int_{-\infty}^{+\infty} g(-\tau)x(\tau)d\tau \tag{S3}$$

becomes

$$\text{filt\_}x(0) = \int_{-\infty}^{+\infty} g(\tau)x(\tau)d\tau \tag{S4}$$

In order to find the dead time of the filter, we want to find the signal width T such that the maximum of filt_$x(t)$, which, as noted above, occurs in this example at $t = 0$, is equal to $A/2$. So the definition of the dead time of the filter, T_{dead}, becomes the condition that when the length of the dwell $T = T_{\text{dead}}$,

$$\text{filt\_}x(0) = \int_{-\infty}^{+\infty} g(\tau)x(\tau)d\tau = \frac{A}{2}, \tag{S5}$$

or

$$\text{filt\_}x(0) = \int_{-\infty}^{+\infty} g(\tau) \cdot A \cdot s_T(\tau)d\tau = \frac{A}{2}. \tag{S6}$$

Note that A can be cancelled from both sides, so the dead time is independent of the signal's amplitude. That is, the dead time of the filter does not depend on the difference in RMS between states.

Since $s_\tau(\tau)$ is zero except between $-T_{\text{dead}}/2$ and $T_{\text{dead}}/2$, Eq. (S6) becomes

$$\int_{-\frac{T_{\text{dead}}}{2}}^{+\frac{T_{\text{dead}}}{2}} g(\tau)d\tau = \frac{1}{2} \tag{S7}$$

where we have already cancelled A from both sides.

Because $g(\tau)$ is a Gaussian, we can rewrite the integral on the left-hand side of Eq. (S7) in terms of the cumulative distribution function of a Gaussian, usually given the variable Φ, where

$$\Phi(x) = \int_{-\infty}^{x} g(t)dt, \tag{S8}$$

and whose solution is given by

$$\int_{-\infty}^{x} g(t)dt = \frac{1}{2}\left[1 + \text{erf}\left(\frac{x}{\sqrt{2}}\right)\right]. \tag{S9}$$

Note that Φ is defined for a Gaussian whose standard deviation is 1; but we are considering a Gaussian with standard deviation σ_g. So when we write the integral in Eq. (S7) in terms of $\Phi(x)$, we must write it as

$$\int_{-\infty}^{\frac{T_{\text{dead}}}{2}} g(\tau)d\tau - \int_{-\infty}^{\frac{-T_{\text{dead}}}{2}} g(\tau)d\tau = \Phi(T_{\text{dead}}/(2\sigma_g)) - \Phi(-T_{\text{dead}}/(2\sigma_g)), \tag{S10}$$

expressing T_{dead} in terms of the σ_g of our filter. Given the solution to $\Phi(x)$ above, we have our final result for the condition on T_{dead},

$$\Phi\left(\frac{T_{\text{dead}}}{2\sigma_g}\right) - \Phi\left(\frac{-T_{\text{dead}}}{2\sigma_g}\right) = \frac{1}{2}\left[1 + \text{erf}\left(\frac{T_{\text{dead}}/(2\sigma_g)}{\sqrt{2}}\right)\right] - \frac{1}{2}\left[1 + \text{erf}\left(\frac{-T_{\text{dead}}/(2\sigma_g)}{\sqrt{2}}\right)\right] = \frac{1}{2}, \tag{S11}$$

which simplifies to

$$\left[\text{erf}\left(\frac{T_{\text{dead}}/(2\sigma_g)}{\sqrt{2}}\right)\right] - \left[\text{erf}\left(\frac{-T_{\text{dead}}/(2\sigma_g)}{\sqrt{2}}\right)\right] = 1. \tag{S12}$$

We can look up that the solution to this expression involving the error function (erf(x)) occurs when $\frac{T_{\text{dead}}}{2\sigma_g} \approx 0.67$, or that

$$T_{\text{dead}} \approx 2 \cdot 0.67 \cdot \sigma_g. \tag{S13}$$

Eq. (S13) gives us an expression for the dead time in terms of the standard deviation of the Gaussian filter that we apply to our data. We apply the filter in Fourier space (such that the process becomes a multiplication between the filter and the Fourier-transformed data, instead of a convolution in time-space). In Fourier space the filter we use has the form

$$G(f) = e^{-0.3466(f/cf_G)^2}. \tag{S14}$$

The factor of 0.3466 in the exponent is chosen to give 3 dB of attenuation at the cutoff frequency (33). That is, when $f = cf_G$, the attenuation is half (3 dB corresponds to a change in power ratio of a factor of 2). For this to be the case, we must have a pre factor in the exponent of $\ln 2/2 = 0.3466$. cf_G is a rescaled cutoff frequency of the filter based on how we define our frequency axis. We choose to establish our frequency axis from −num. frames/2 to +num. frames/2, where "num. frames" is the number of image frames in a trajectory. If we want a cutoff frequency for the filter at f_{cG} Hz, then we must define

$$cf_G = \frac{\text{num. frames}}{fps \times f_{cG}^{-1}}, \tag{S15}$$

where fps is the frame rate of the camera (30 Hz in our case). This is essentially a unit conversion, since our frequency axis is unitless but f_{cG} is in Hz. This conversion coincides with the convention of the Matlab fft command (by which we Fourier transform our data), which returns a vector the same length as the input vector, in frequencies from 0 to $fps/2$.

The Fourier transform of a Gaussian is a Gaussian, so in time space the Gaussian filter defined in Eq. (S14) becomes

$$g(t) = \frac{1}{\sqrt{2\pi}\sigma_g} e^{-\frac{t^2}{2\sigma_g^2}}, \tag{S16}$$

where σ_g defines the width of the filter and is related to f_{cG} by (33)

$$\sigma_g = \frac{\sqrt{\ln 2}}{2\pi f_{cG}}. \tag{S17}$$

We use $f_{cG} = 0.0326$ Hz, which corresponds to a Gaussian-shaped smoothing profile with a 4 second standard deviation in time space. Given this 0.0326 Hz cutoff frequency, according to Eq. (S13) we calculate that the dead time of our filter is 5.5 seconds.

S1.4 Fitting data of lifetimes versus J-factors.

Fitting was performed using the built-in lsqnonlin function in Matlab, with the standard errors on the mean lifetimes as the weights. Individual data sets (unlooped state vs. looped state, and data flanked by O_{id}-O_1 vs. O_{id}-O_2) were fit to a generic power law of the form $\langle\tau\rangle = a \times J_{loop}^b$, or all four data sets (the two state and the two pairs of flanking operators) were fit simultaneously to Eqs. S75 amd S76 in Sec. S2.3.4. That is, for the global fit to all four data sets below, the m parameter was forced to be the same for all four data sets, but the proportionality constant was allowed to vary between data sets.

As in (1), we believe that the largest source of error in the data is the variability between tethers; therefore, as in (1), errors on the fit parameters were calculated according to a bootstrapping scheme, in which the trajectories that comprise each data set were resampled with replacement 10,000 times, and from these resampled sets, 10,000 new mean lifetimes, standard errors on the lifetimes, and J-factors were computed. The fits were then redone 10,000 times using these new mean lifetimes and J-factors, and the errors on the fit parameters taken to be the standard errors of the 10,000 new fit parameters. The fit parameters and their errors we obtain for the additional data are in reasonable agreement with that of Fig. 3 in the main text.

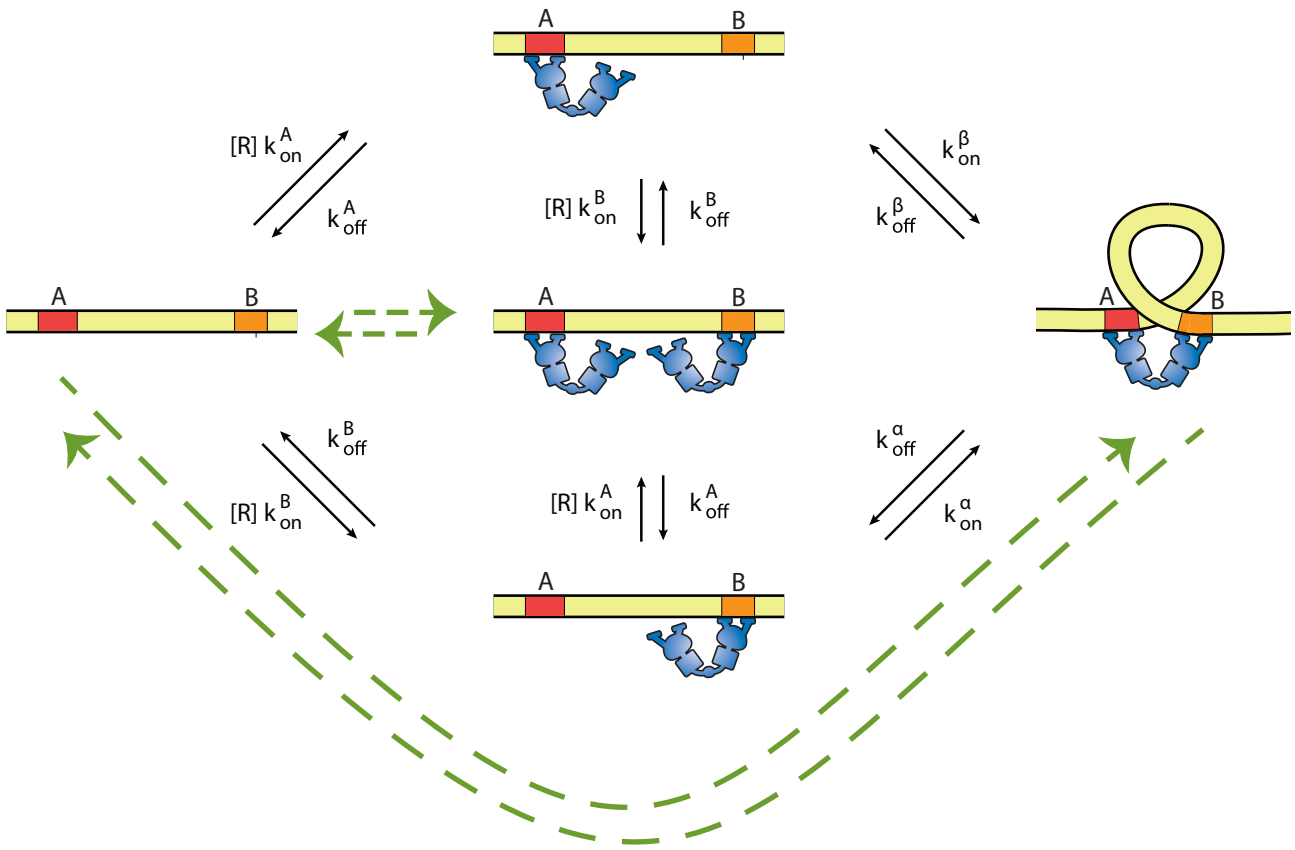

Figure S2: **Kinetic scheme for looping.** In thermal equilibrium, for a DNA (yellow line) with two Lac repressor binding sites A and B (orange and red boxes) exposed to a solution of Lac repressor molecules (blue shapes), the system transitions between the four unlooped states and the looped state discussed in the text. Kinetic rates governing each transition are labeled above the arrows indicating that transition. Each transition is either first-order (characterized by one rate constant k with unit $\frac{1}{time}$) or pseudo-first-order (characterized by a rate $[R]k$ with units $\frac{1}{time}$). We assume that the concentration of repressor is much larger than the concentrations of its binding sites, such that the concentration of free repressor in solution is effectively constant over the course of the experiment (see (1) for details and a discussion of when this assumption breaks down). Therefore the second-order binding steps of the form $R + A \rightarrow RA$ can be simplified to pseudo-first-order. Examples for the forbidden pathways discussed in (iv) are shown in green arrows.

S2 Supplementary Methods: Theoretical Analysis

In these sections we describe in detail the kinetics scheme we introduce in the main text, and give a fuller account of its reconciliation with our experimental results.

S2.1 Kinetics scheme for protein-mediated looping.

S2.1.1 States of the looping system and assumptions in our derivation.

We start by setting up some basic parameters of the system and stating some assumptions required for our derivation. As described in our previous work in which we derived a statistical mechanical model for the probability of loop formation by the Lac repressor (1, 24), our system can adopt five coarse-grained states, illustrated in Fig. S2: no protein bound on DNA, either operator (i.e. binding site) A or B being

bound, both operators bound, and the looped state. Their relative statistical weights are given by

$$w_0 = 1, \tag{S18}$$

$$w_{A-bound} = \frac{[R]}{K_A}, \tag{S19}$$

$$w_{B-bound} = \frac{[R]}{K_B}, \tag{S20}$$

$$w_{AB} = \frac{[R]^2}{K_A K_B}, \tag{S21}$$

$$w_{loop} = \frac{[R] J_{loop}}{2 K_A K_B}. \tag{S22}$$

The relationship between the looping probabilities measured in TPM, p_{loop}, the repressor-operator dissociation constants for the two operators that flank the loop, K_A and K_B, and the looping J-factor of the DNA in the loop, J_{loop}, can be described as

$$p_{loop} = \frac{w_{loop}}{w_0 + w_{A-bound} + w_{B-bound} + w_{AB} + w_{loop}} \tag{S23}$$

$$= \frac{\frac{[R] J_{loop}}{2 K_A K_B}}{1 + \frac{[R]}{K_A} + \frac{[R]}{K_B} + \frac{[R]^2}{K_A K_B} + \frac{[R] J_{loop}}{2 K_A K_B}}. \tag{S24}$$

where $[R]$ is the concentration of Lac repressor. J_{loop} is related to the looping free energy by $J_{loop} = 1\text{ M}\ e^{-\beta \Delta F}$. "1 M" is the standard state calculated by discretizing the solution volume to molecular size lattice and the exponential factor is the occupation number given by Boltzmann distribution. K_A, K_B and $[R]$ are also in molar. Generally, the "looping free energy" contains contributions from the bending, twisting energy change and entropic change from both the DNA and the protein. Figure S2 summarizes our kinetic model for the transition state theory. We use several simplifications as follows.

(*i*) We assume that two LacI binding to operator A and B are independent, although we know the binding of LacI does bend the operators and has a small effect on the tether RMS (as reported in (1)), and in principle binding of two LacI could couple. (Some researchers discussed protein-protein coupling through both binding to DNA.)

(*ii*) We assume at all the LacI concentrations we work with, there is negligible nonspecific binding of LacI to DNA. In fact, the dissociation constant of the LacI for its specific binding sites (operators) is about 10^{-9} times smaller than non-specific binding (35). The dissociation constant for non-specific binding is in the $10^{-5}M$ range, which is much higher than the highest repressor concentration we use ($10^{-8}M$). Non-specific binding, if it occurred, might shorten the DNA tethers and result in higher local concentration of adsorbed LacI available to bind to DNA. Ref. (36) reported that nonspecific binding of phage Lambda cI protein to DNA shortens loop length and broadens its distribution in a concentration-dependent manner. This also changes and broadens the observed k_{on} and k_{off} of cI to an operator (which are supposed to be independent of cI concentration). However, in our system the shortening of tether by protein binding is small and is not concentration dependent, as shown in (1). Our LacI looping system therefore does not suffer from non-specific binding at the concentrations we work with, and we do not need concentration-dependent correction terms for the rate constants.

(*iii*) No depletion of LacI from the solution. In our experiments, LacI is present in excess over the DNA, so the LacI concentration in solution is essentially constant. Hence, the second-order reaction of a repressor binding to an operator (for example, $R + A \rightarrow RA$) becomes a pseudo-first-order reaction. All

the reaction steps in Figure S2 are thus first-order or pseudo-first-order reactions.

The above assumptions were also used in the statistical mechanical model for looping probability (see further discussion of these issues in (1)). The observed looping probabilities fit well to this statistical mechanical model (see Ref. (1)), and gives us confidence that assumptions (*i*), (*ii*) and (*iii*) are indeed valid for our experimental conditions. We next consider the kinetics that govern the transition among these states and adopt a few assumptions commonly used in chemical kinetics analysis.

(*iv*) We assume transitions occur at one molecular junction at a time (with the probability of order $k\delta t$, where k is a reaction rate and δt is an infinitesimal time interval). Simultaneous actions at two junctions would be very unlikely (because for two events to happen at the same time the probability would be of order $kk'(\delta t)^2$). For example, the probability of both heads of LacI grabbing the operators simultaneously while the loop forms is negligible. One of its ends always has to bind first and wait for the polymer fluctuation to bring the other end close to the other operator. Similarly, two LacI binding to two operators simultaneously is a process of negligible significance. The same is true for simultaneous dissociation at two junctions or any other high-order transitions. The two example forbidden pathways are shown in Figure S2 in green arrows.

(*v*) As discussed in Sec. S1.2 and Fig. S1 above, with TPM we actually observe two different looped states, with distinct RMS values, that we call the "bottom" and "middle" looped states. They are likely looped states with different geometries and they may interconvert (see Ref. (30)). However, for the most part here we consider only the coarse-grained total looped state, because, as described in Ref. (2), the bottom state is rare, and we do not have much data on bottom state lifetimes for most constructs. Hence, our kinetic analysis focuses on the switching rates between the unlooped state and the dominant looped state.

S2.1.2 Master equations.

From the kinetics pathways shown in Figure S2, the master equations of the system are given by

$$\frac{dp_0}{dt} = -([R]k^A_{on})p_0 + k^A_{off}p_{A-bound} - ([R]k^B_{on})p_0 + k^B_{off}p_{B-bound}, \tag{S25}$$

$$\frac{dp_{A-bound}}{dt} = -(k^A_{off} + [R]k^B_{on} + k^\beta_{on})p_{A-bound} + [R]k^A_{on}p_0 + k^B_{off}p_{AB} + k^\beta_{off}p_{loop}, \tag{S26}$$

$$\frac{dp_{B-bound}}{dt} = -(k^B_{off} + [R]k^A_{on} + k^\alpha_{on})p_{B-bound} + [R]k^B_{on}p_0 + k^A_{off}p_{AB} + k^\alpha_{off}p_{loop}, \tag{S27}$$

$$\frac{dp_{AB}}{dt} = -(k^A_{off} + k^B_{off})p_{AB} + [R]k^A_{on}p_{A-bound} + [R]k^B_{on}p_{B-bound}, \tag{S28}$$

$$\tag{S29}$$

and

$$\frac{dp_{loop}}{dt} = -k^\beta_{off}p_{loop} + k^\beta_{on}p_{A-bound} - k^\alpha_{off}p_{loop} + k^\alpha_{on}p_{B-bound}. \tag{S30}$$

These probabilities must add up to one, that is,

$$p_0 + p_{loop} + p_{AB} + p_{A-bound} + p_{B-bound} = 1. \tag{S31}$$

S2.1.3 Application of detailed balance.

Before turning to a derivation of expressions for average lifetimes in terms of the rate constants in Fig. S2 and Fig. S2, we next establish some basic relationships between the statistical weights introduced in the previous section and the kinetic parameters in Fig. S2, which will be used in the next section.

In Fig. S2, k_{on}^{α}, k_{off}^{α} represent the on and off rate constants for LacI to bind to and dissociate from operator A, when its other end is bound to operator B. Similarly, k_{on}^{β}, k_{off}^{β} represent the on and off rate constants for operator B when the Lac repressor already binds to A with one end. As discussed above, we assume all the reaction steps are first-order or pseudo-first-order, so the units of k_{on}^{α}, k_{off}^{α}, k_{on}^{β}, k_{off}^{β}, k_{off}^{A}, k_{off}^{B} and $[R]k_{on}^{A}$, $[R]k_{on}^{B}$ are $\frac{1}{[time]}$. Because of DNA looping, we expect the Lac repressor on rates to operator A and B, k_{on}^{α} and k_{on}^{β}, to differ from the original on rates $[R]k_{on}^{A}$ and $[R]k_{on}^{B}$. In earlier work, J_{loop} was used interchangeably with the *effective* local concentration of LacI (37). If we consider the looping reaction at operator A when the LacI has already bound to other site B, in the usual sense of intermolecular binding using an effective protein concentration $[I]$, we can write the reaction as $I + B - bound \rightarrow looping$, while the usual binding reaction of LacI onto site A is $R + A \rightarrow RA$. Making use of the statistical weights given in Eq. S18, S19, S20 and S22, the relative amount of the different species in these reactions are

$$\frac{[looping]}{[B-bound]} = \frac{w_{loop}}{w_{B-bound}} = \frac{J_{loop}}{2K_A}, \tag{S32}$$

and

$$\frac{[RA]}{[A]} = \frac{w_{A-bound}}{w_0} = \frac{[R]}{K_A}. \tag{S33}$$

Hence, we can identify $[I]$ with $\frac{J_{loop}}{2}$. This is why the looping J-factor is usually considered an effective repressor concentration.

J_{loop} affects how easily the empty site could find a repressor molecule in its close proximity. A large J_{loop} means that when one hand of the repressor is bound to one site, it is more easily brought to the other site because it is coupled to the DNA. Hence, the on rates k_{on}^{α} and k_{on}^{β}, which depend upon the chance for the operator to see a LacI when the other end of of the LacI has already bound to the other operator, should be regulated by the dynamics and strain of DNA loop formation. Indeed, loop formation kinetics have been modeled by diffusion in an effective energy landscape which is governed by the polymer stiffness and size (38–41). On the other hand, the off rates k_{off}^{α} and k_{off}^{β} are in general difficult to model despite various efforts in the literature, because the detailed dynamical atomic position, orientation and electrostatic interactions (coupled by solvent) are not known. Here we do not exclude the possibility that the off rates k_{off}^{α} and k_{off}^{β} are also dependent on J_{loop} and are different from k_{off}^{A} and k_{off}^{B} as well.

If we look at the transitions between operator B being bound and the looped state, we can write down detailed balance as

$$k_{on}^{\alpha} \cdot p_{B-bound} = k_{off}^{\alpha} \cdot p_{loop}. \tag{S34}$$

Similarly, between operator A being bound and the looped state, detailed balance says

$$k_{on}^{\beta} \cdot p_{A-bound} = k_{off}^{\beta} \cdot p_{loop}. \tag{S35}$$

Inserting the statistical weights from Eq. S19, S20, and S22 to the above detailed balance relations leads to

$$\frac{k_{on}^{\alpha}}{k_{off}^{\alpha}} = \frac{p_{loop}}{p_{B-bound}} = \frac{w_{loop}}{w_{B-bound}} = \frac{\frac{[R]J_{loop}}{2K_AK_B}}{\frac{[R]}{K_B}} = \frac{J_{loop}}{2K_A}, \tag{S36}$$

and

$$\frac{k_{on}^{\beta}}{k_{off}^{\beta}} = \frac{p_{loop}}{p_{A-bound}} = \frac{w_{loop}}{w_{A-bound}} = \frac{\frac{[R]J_{loop}}{2K_AK_B}}{\frac{[R]}{K_A}} = \frac{J_{loop}}{2K_B}. \tag{S37}$$

On the other hand, we can also relate the dissociation constants K_A and K_B to the kinetic rate constants. The detailed balance between the state with nothing bound on DNA and operator A bound by one Lac repressor is

$$([R]k_{on}^{A}) \cdot p_0 = k_{off}^{A} \cdot p_{A-bound}. \tag{S38}$$

The dissociation constant K_A by definition is the ratio of concentrations $\frac{[R][A]}{[RA]}$ for the reaction $R + A \rightleftharpoons RA$. Since $\frac{[A]}{[RA]}$ is just $\frac{p_0}{p_{A-bound}}$, K_A is given by

$$K_A = \frac{[R]p_0}{p_{A-bound}} = \frac{k_{off}^{A}}{k_{on}^{A}}. \tag{S39}$$

Similarly, the detailed balance between the state with nothing bound on DNA and operator B bound by one Lac repressor is

$$([R]k_{on}^{B}) \cdot p_0 = k_{off}^{B} \cdot p_{B-bound}. \tag{S40}$$

Thus K_B has the form

$$K_B = \frac{[R]p_0}{p_{B-bound}} = \frac{k_{off}^{B}}{k_{on}^{B}}. \tag{S41}$$

S2.1.4 Associate the average lifetimes with rate constants.

Experimentally we cannot distinguish the four unlooped states because they yield similar RMS values. What are experimentally observable are the lifetimes of the looped state and the unlooped state. For each construct (specified by loop sequence, length and operators), measured at a particular LacI concentration, we therefore obtain distributions of the *Looped* lifetimes $p(\tau_{looped})$ and the *Unlooped* lifetimes $p(\tau_{unlooped})$, which give average lifetimes $< \tau_{looped} >$ and $< \tau_{unlooped} >$ for each construct, as well as looping probabilities, p_{loop}, which are the total time spent in the looped state divided by the total observation time. Because the system is either in the looped or unlooped state, the total time spent in each state, as well as the average lifetime spent in each state, are by definition associated with the probability in each state and are given by

$$\frac{< \tau_{looped} >}{< \tau_{unlooped} >} = \frac{p_{loop}}{1 - p_{loop}} = \frac{w_{loop}}{w_0 + w_{A-bound} + w_{B-bound} + w_{AB}} \tag{S42}$$

$$= \frac{\frac{[R]J_{loop}}{2K_AK_B}}{1 + \frac{[R]}{K_A} + \frac{[R]}{K_B} + \frac{[R]^2}{K_AK_B}} \propto J_{loop}. \tag{S43}$$

We will try to connect the rate constants in the model (because the rate constants are useful when we talk about transition state theory later) to the experimentally observed lifetimes. From the looped state to the unlooped states there are two paths, determined by rate constants k_{off}^{α} and k_{off}^{β}. The lifetime distribution assuming a one-step Poisson process (see (42) for an ion channel example) is

$$p(\tau_{looped}) = (k_{off}^{\alpha} + k_{off}^{\beta}) e^{-(k_{off}^{\alpha} + k_{off}^{\beta})\tau_{looped}}. \tag{S44}$$

Hence the average looped lifetime is

$$< \tau_{looped} > = \frac{1}{(k_{off}^{\alpha} + k_{off}^{\beta})}. \tag{S45}$$

Now, if the unlooped state is truly one single state, the average unlooped lifetime would be

$$< \tau_{unlooped} >^{single\ state} = \frac{1}{(k_{on}^{\alpha} + k_{on}^{\beta})}. \tag{S46}$$

The experimentally observed average lifetime has an inverse relationship with the rate constants. Moreover, this inverse relationship actually still holds, up to some proportionality constants, even when the state is composed of multiple microstates. To show this is the case, we return to the statement above that the unlooped state involves four indistinguishable states in TPM. Looking at Figure S2 we know that if the system starts within any of the four unlooped states, before it reaches the looped state, it can only follow the arrows with the these rate constants: k_{on}^{α}, k_{on}^{β}, $[R]k_{on}^{A}$, $[R]k_{on}^{B}$, k_{off}^{A}, k_{off}^{B}. Hence, we know only these rate constants will appear in the functional form of the unlooped lifetime distribution, even though we do not know the analytical solution. In other words,

$$p(\tau_{unlooped}) = \text{Function}(k_{on}^{\alpha}, k_{on}^{\beta}, [R]k_{on}^{A}, [R]k_{on}^{B}, k_{off}^{A}, k_{off}^{B}). \tag{S47}$$

We next make use of the fact that lifetimes are associated with the looping probabilities to derive an expression for the average unlooped lifetime, by combining Eqs. S43, S54, S36, and S37 as follows. Starting from Eq. S43, $< \tau_{unlooped} >$ can be written as

$$< \tau_{unlooped} >=< \tau_{looped} > \frac{1 + \frac{[R]}{K_A} + \frac{[R]}{K_B} + \frac{[R]^2}{K_A K_B}}{\frac{[R] J_{loop}}{2K_A K_B}}. \tag{S48}$$

We then plug in the expression of $< \tau_{looped} >$ given by Eq. S54 to the expression of $< \tau_{unlooped} >$ above and obtain

$$< \tau_{unlooped} >= \frac{1}{(k_{off}^{\alpha} + k_{off}^{\beta})} \frac{1 + \frac{[R]}{K_A} + \frac{[R]}{K_B} + \frac{[R]^2}{K_A K_B}}{\frac{[R] J_{loop}}{2K_A K_B}} \tag{S49}$$

$$= \frac{1 + \frac{[R]}{K_A} + \frac{[R]}{K_B} + \frac{[R]^2}{K_A K_B}}{(\frac{J_{loop} k_{off}^{\alpha}}{2K_A})(\frac{[R]}{K_B}) + (\frac{J_{loop} k_{off}^{\beta}}{2K_B})(\frac{[R]}{K_A})} \tag{S50}$$

Next, we can use use the detailed balance relations for the α and β rate constants given by Eq. S36 and Eq. S37 and arrive at

$$< \tau_{unlooped} >= \frac{1 + \frac{[R]}{K_A} + \frac{[R]}{K_B} + \frac{[R]^2}{K_A K_B}}{(k_{on}^{\alpha})(\frac{[R]}{K_B}) + (k_{on}^{\beta})(\frac{[R]}{K_A})}. \tag{S51}$$

Then we multiply both dividend and divisor with the factor $\frac{K_A K_B}{[R]^2}$ and arrive at the form

$$< \tau_{unlooped} >= \frac{\frac{K_A K_B}{[R]^2} + \frac{K_B}{[R]} + \frac{K_A}{[R]} + 1}{k_{on}^{\alpha} \frac{K_A}{[R]} + k_{on}^{\beta} \frac{K_B}{[R]}} = \frac{(1 + \frac{K_A}{[R]})(1 + \frac{K_B}{[R]})}{k_{on}^{\alpha} \frac{K_A}{[R]} + k_{on}^{\beta} \frac{K_B}{[R]}}. \tag{S52}$$

We can also replace K_A and K_B with kinetic rate constants given in Eq. S39 and Eq. S41 and obtain

$$< \tau_{unlooped} >= \frac{(1 + \frac{k_{off}^{A}}{[R]k_{on}^{A}})(1 + \frac{k_{off}^{B}}{[R]k_{on}^{B}})}{k_{on}^{\alpha}(\frac{k_{off}^{A}}{[R]k_{on}^{A}}) + k_{on}^{\beta}(\frac{k_{off}^{B}}{[R]k_{on}^{B}})}. \tag{S53}$$

We see that indeed $< \tau_{unlooped} >$ can be expressed in terms of only the set of parameters k_{on}^{α}, k_{on}^{β}, $[R]k_{on}^{A}$, $[R]k_{on}^{B}$, k_{off}^{A}, k_{off}^{B}. Also, even though we do not have an analytical solution for the probability distribution of the unlooped lifetime, and this expression we have for the average unlooped lifetime $< \tau_{unlooped} >$ is redundant, we confirm that it is inversely proportional to k_{on}^{α} and k_{on}^{β}. This inverse proportionality between average lifetime and the rate constants is all we need when we apply transition state theory (which predicts the rate constants' dependence on the looping J-factor) to explain the power-law-like dependence of lifetimes on J-factor.

S2.2 The Concentration Dependence of Kinetics.

Having established a basic framework for the relationships between average lifetimes, repressor concentration, looping probabilities, and rate constants, we next turn to a comparison between our experimental results and our theoretical framework, starting with experimental observations of the dependence of the average lifetime on repressor concentration.

The effects of repressor concentration and flanking operator affinity on looped and unlooped lifetimes are shown in Fig. S3. Based on the kinetic scheme in Fig. 2 and the definition of p_{loop}, the loop breakdown rates k^{α}_{off} and k^{β}_{off} are related to the experimentally observed mean looped lifetime $\langle \tau_{looped} \rangle$ by

$$\langle \tau_{looped} \rangle = \frac{1}{\left(k^{\alpha}_{off} + k^{\beta}_{off} \right)}. \tag{S54}$$

The loop formation rates k^{α}_{on} and k^{β}_{on} are related to the mean unlooped lifetime $\langle \tau_{unlooped} \rangle$ by

$$\langle \tau_{unlooped} \rangle = \frac{\left(1 + \frac{k^{A}_{off}}{[R] k^{A}_{on}} \right) \left(1 + \frac{k^{B}_{off}}{[R] k^{B}_{on}} \right)}{k^{\alpha}_{on} \frac{k^{A}_{off}}{[R] k^{A}_{on}} + k^{\beta}_{on} \frac{k^{B}_{off}}{[R] k^{B}_{on}}} \tag{S55}$$

$$= \langle \tau_{looped} \rangle \left(\frac{1}{p_{loop}([R])} - 1 \right). \tag{S56}$$

S2.2.1 Looped state lifetimes are independent of repressor concentration.

According to Eq. S54, $< \tau_{looped} >= \frac{1}{(k^{\alpha}_{off} + k^{\beta}_{off})}$. Also, both rate constants k^{α}_{off} and k^{β}_{off} are determined by DNA-protein interaction and are independent of $[R]$. As a result, the looped state lifetimes should exhibit no dependence on repressor concentration $[R]$. As shown in Fig. S3b, our data are reasonably consistent with this prediction.

The value of $< \tau_{looped} >$ does depend on operator binding site identity, however: the four constructs have one common binding site (say they have the same k^{β}_{off}), so the values of $< \tau_{looped} >$ will depend on the different k^{α}_{off}. We see that from Figure S3b, constructs with stronger binding sites have longer $< \tau_{looped} >$ and hence smaller k^{α}_{off}. (The order of LacI-operator binding affinities is $O_{id} > O_1 > O_2$.) As we will see in section S2.3.2 in Eq. S66, there is a $e^{-\beta E_A}$ term in k^{α}_{off}. This could possibly qualitatively explain why construct with stronger binding site (bigger E_A, here we use positive values of binding energies) would have smaller k^{α}_{off}. However, we do not know the pre-factors for different constructs, and we do not have a definitive model to predict the operator dependence of rate constants, so we cannot conclude definitively that this $e^{-\beta E_A}$ term is the source of the variation in average lifetime between constructs.

S2.2.2 The unlooped lifetime depends on repressor concentration via a shifted equilibrium.

On the other hand, the unlooped lifetime given by Eq. (S55) does depend on $[R]$, and in this case the data shown in Fig. S3a is consistent with the predicted $[R]$ dependence. Briefly, the shape of this dependence on R is consistent with the prediction of Eq. S56: since $\langle \tau_{looped} \rangle$ is $[R]$-independent, the $[R]$-dependence of $\langle \tau_{unlooped} \rangle$ comes from the $[R]$-dependence in the looping probability and is captured by the ratio of unlooped and looped probabilities, or the "relative unlooped frequency" $\frac{1}{p_{loop}([R])} - 1 \equiv \omega$ in Eq. (S56) as explained below. That is, $\langle \tau_{unlooped} \rangle$ should scale linearly with ω, as shown in Fig. S3c.

The unlooped lifetime depends on $[R]$ as shown in Figure S3a. We can explain this dependency by

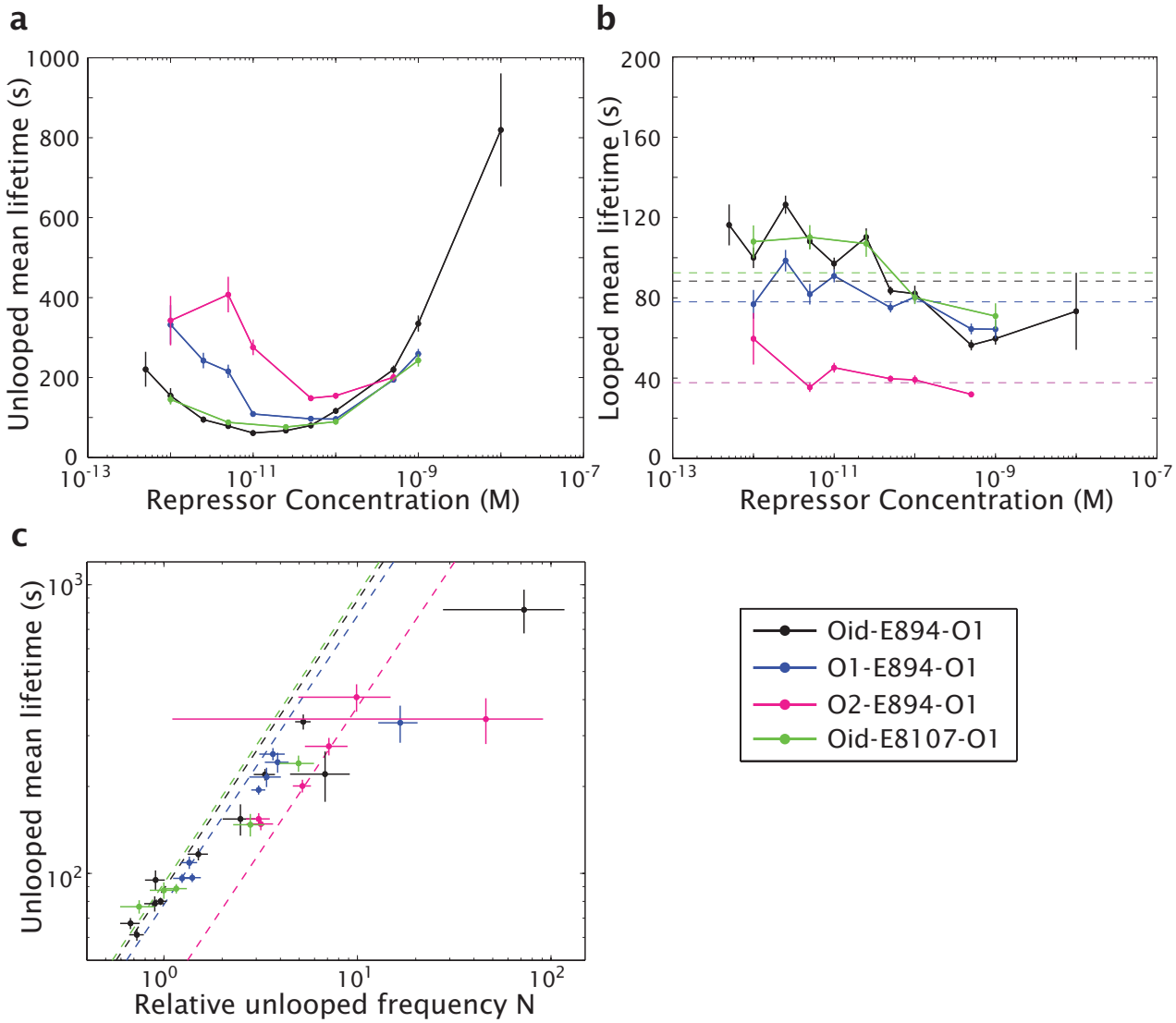

Figure S3: **Mean state lifetime as a function of repressor concentration and flanking operators**. All of these constructs contain the E8 sequence in the loop, but two (black and green) have the same flanking operators but different loop lengths, while the rest have the same loop length as the black data but different flanking operators. Naming convention details are given in the Methods. **a,** Mean unlooped state lifetimes versus repressor concentration $[R]$. **b,** Mean looped state lifetimes versus repressor concentration. Horizontal dashed lines represent the average looped state lifetime over all concentrations for a particular construct, weighted by the error at each concentration. As discussed in the text, the mean lifetime of the looped state should be invariant with concentration; see also Fig. S4 and Sec. S3.1 below. **c,** Mean unlooped state lifetimes versus the relative unlooped frequency ω, defined as the term that multiplies $\langle \tau_{looped} \rangle$ in Eq. (S56). The minimum unlooped mean lifetime for each construct in panel **a** corresponds to the minimal relative unlooped frequency and maximal looping probability. Dashed lines show $\langle \tau_{unlooped} \rangle = b * \omega$, with slope b for each construct corresponding to the weighted-average looped state lifetimes shown as horizontal dashed lines in panel **b**. Given the relationship between $\langle \tau_{unlooped} \rangle$ and ω derived in Eq. (S56), which predicts a linear relationship with a slope corresponding to the mean looped state lifetime, the dashed lines in this panel are therefore a parameter-free "fit" demonstrating that the relationship between $\langle \tau_{unlooped} \rangle$, $\langle \tau_{looped} \rangle$ and ω are in good agreement with the predictions of our model.

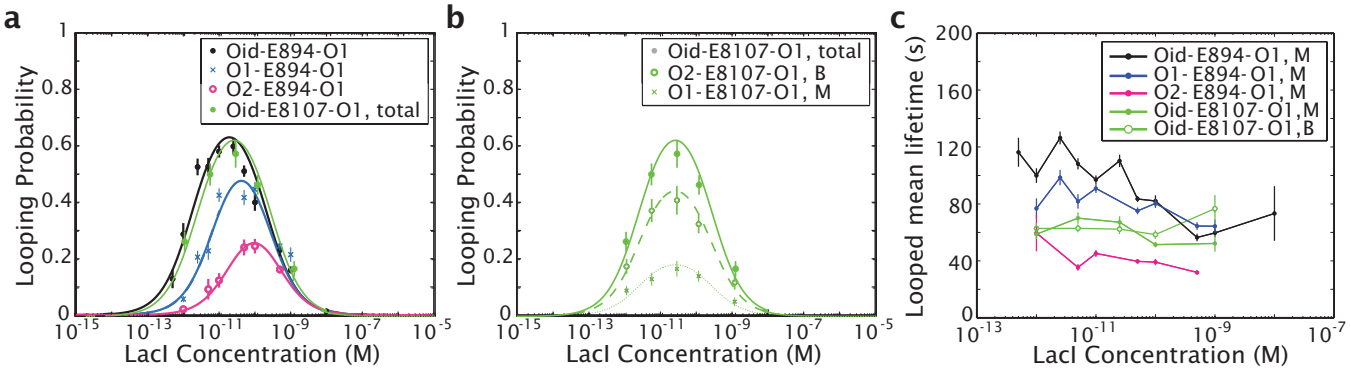

Figure S4: **Looping probability (a,b) and looping dwell time (c) as a function of repressor concentration.** Data in **a, b** are mean looping probabilities and are adapted from (1); errors are standard errors on the mean. Curves are fits to our statistical mechanical model (see Eq. S24) with J_{loop}, K_A and K_B for each sequence as the fit parameters. Note that the two constructs represented by filled circles have the same flanking operators but different loop lengths; the other constructs have the same loop length and sequence as the black data but have different flanking operators. The difference between **a** and **b** is that **b** shows the looping probabilities for the two looped states, the "middle" (M) and "bottom" (B) states described in Sec. S1.2 above, for the one of these four constructs that has both states. The other three constructs shown in **a** have only the "middle" state. In **c**, the mean dwell times of the looped states whose probabilities are shown in **a, b** are plotted. Data are the same as in Fig. S3 above, except here we have plotted the dwell times of the two looped states of the Oid-E8107-O1 construct separately. Note that when the dwell times of the two states are plotted separately, the invariance with repressor concentration that our theoretical framework predicts is more clear. It is possible, then, that the looped state in the Oid-E894-O1 (and possibly that of O1-E894-O1 as well), which appears as a single tether length in our data, is in fact composed of different microstates, which, if plotted separately, would then appear invariant with concentration. This hypothesis is supported by the fact that the distributions of the looped state dwell times whose mean values are plotted here are not singly exponentially distributed (see Fig. S8 below), and by the conclusions of the vb-HMM analysis mentioned in Sec. S1.2 above (see Ref. (30)).

Eq. S55,

$$< \tau_{unlooped} >= \frac{(1+\frac{k^A_{off}}{[R]k^A_{on}})(1+\frac{k^B_{off}}{[R]k^B_{on}})}{k^{\alpha}_{on}(\frac{k^A_{off}}{[R]k^A_{on}})+k^{\beta}_{on}(\frac{k^B_{off}}{[R]k^B_{on}})}. \tag{S57}$$

We expect all the rate constants k's to be independent of repressor concentration $[R]$ (because they are determined by local interactions between molecules and will not be affected by other repressor molecules present in the system). However, $< \tau_{unlooped} >$ depends on $[R]$ explicitly. $[R]$ shifts the equilibrium among the internal unlooped states—if we look at the looping probability as a function of repressor concentration, given in Figure S4, we see some similarity between it and Figure S3a.

We do not know the rate constants in Eq. S57, but it is identical to Eq. S48 which says

$$< \tau_{unlooped} >=< \tau_{looped} > \frac{1+\frac{[R]}{K_A}+\frac{[R]}{K_B}+\frac{[R]^2}{K_AK_B}}{\frac{[R]J_{loop}}{2K_AK_B}}. \tag{S58}$$

Since the values of K_A, K_B and J_{loop} are constants for each construct, and also we know that $< \tau_{looped} >$ is independent of $[R]$, this tells us how $< \tau_{unlooped} >$ depends on $[R]$.

Compare Eq. S58 with looping probability given in Eq. S24, we see that the way $< \tau_{unlooped} >$ depend on $[R]$ is entirely governed by how p_{loop} depend on $[R]$. The repressor concentration $[R]$ shifts the equilibrium and hence controls the looping probability and the unlooped lifetime. We can rewrite Eq. S58 in the form

$$< \tau_{unlooped} >=< \tau_{looped} > \frac{1+\frac{[R]}{K_A}+\frac{[R]}{K_B}+\frac{[R]^2}{K_AK_B}}{\frac{[R]J_{loop}}{2K_AK_B}} =< \tau_{looped} > (\frac{1}{p_{loop}([R])}-1). \tag{S59}$$

Since $< \tau_{looped} >$ is constant over $[R]$, $< \tau_{unlooped} >$ should scale as $\frac{1}{p_{loop}([R])} - 1 = \frac{p_{unlooped}([R])}{p_{loop}([R])} \equiv \omega$. We compute this relative unlooped frequency ω, *i.e.* the odds of being in the unlooped state, from the measured looping probabilities given in Figure S4, with the errors on ω calculated using our standard bootstrapping procedure (see (1) and Sec. S1.4 above), and show in Figure S3c that $< \tau_{unlooped} >$ and ω indeed are correlated linearly.

S2.3 The J-factor Dependence of Kinetics.

S2.3.1 Looped and unlooped lifetimes scale with looping J-factor.

Figure 3 in the main text show the lifetimes plotted as a function of looping J-factors. We see that $< \tau_{looped} >$ and $< \tau_{unlooped} >$ both scale with J_{loop}, without loop *sequence* or *helical period* dependence, despite the fact that the looping boundary conditions are different for the sequences we measured. (When looping probabilities are close to 0 or when J-factor is small, the state transition events are rare. Less lifetime data is available from the same amount of total observation time and the average lifetimes will have bigger error bars.) The two plots shown in Figure 3a,b show opposite trends in looped lifetime and unlooped lifetime with respect to the looping J-factor. Comparing the trends in Figure 3a,b with those in Figure S3a,b, we see that the interpretation of J_{loop} as effective repressor concentration fails to capture the opposite dependencies of looped and unlooped lifetimes with J_{loop}.

It is especially intriguing that not only loop formation kinetics, but also loop breakdown kinetics, are controlled by the looping J-factor, which is a function of DNA and protein bending and torsional flexibilities and the geometry of these polymers. The kinetics of loop formation are usually modeled by diffusion in a one-dimensional energy landscape governed by the polymer stiffness (38–41), from which the first passage time from unlooped to looped state is calculated. Hence, it is not surprising that the loop formation process is dependent on the J-factor, which is a function of DNA flexibility. On the other hand, the loop breakdown process is less addressed and the off rate constants of chemical reactions are usually considered to be only dependent on *local* bimolecular interaction strength, which can be tuned by ionic concentration and temperature in the environment. It is surprising that our data reveals that the *long-distance* DNA looping plays a role in the loop breakdown process. The DNA looping system gives an novel example where both on and off rate constants are modulated by the same, action-at-a-distance mechanical quantity. We will try to explain this scaling in the following arguments.

S2.3.2 Transition state theory.

We use transition state theory to phenomenologically model the fact that both looped and unlooped lifetimes are dependent on J_{loop}, and that $< \tau_{looped} >$ and $< \tau_{unlooped} >$ have opposite trends with respect to J_{loop}. Transition state theory in chemical kinetics assumes a transition state with a higher energy between the initial and final states of the reaction. The transition state is short-lived and its detailed conformation and energy are usually unknown. (First-principle simulations can be helpful in obtaining information about the structure and free energy of the transition state, and have been attempted for protein-mediated looping. However, in the case of repressor-mediated DNA looping, the boundary conditions of the loop are not yet well-established, so simulations of the looping J-factor can yield quite diverse results, depending on the assumptions made about these boundary conditions (1). On the other hand, in the case of ligase-mediated DNA cyclization, there is an exact solution for the free energy of the cyclized DNA because the boundary conditions are well-defined, and we expect the transition state for cyclization reactions to be easier to model than repressor-mediated looping. The same lifetime scaling with free energy should hold true for the opening and closure dynamics in cyclization, and could serve as a way to check the simulated transition state free energy.)

If the activation energy of a path is E_{act}, the rate constant would have the form $k = k_0 e^{-\beta E_{act}}$. k_0 is determined by the detailed atomic orientations and the short-ranged electrostatic interactions of the molecules. In principle, the forward and reverse paths and the transition states for them do not need to be

the same, but in this case of looping and unlooping, assuming the same forward and reverse paths would be the first order approximation. In fact, as will be seen below, the assumption that the forward and reverse reactions follow the same path naturally explains both dependencies of the looped and unlooped lifetimes to the looping J-factors.

We summarize our hypothesized free energy landscape in Figure 2c in the main text. From the dissociation constants K_A and K_B we can obtain E_A and E_B, the binding energy of the LacI molecule to the operators A and B. In Figure 2c, we consider the transition between the state in which only binding site A is bound by LacI, and the looped state. We denote $\Delta F^{\ddagger}_{loop}$ as the configurational free energy change to the highly distorted DNA and possibly also bending of the Lac repressor in the transition state. (Ref. (13) suggests that the Lac repressor itself has configurational change during looping). The free energy of the unlooped, looped and the transition states are thus given by

$$F_{unlooped} = -E_A + F_0. \tag{S60}$$

$$F_{looped} = -E_A - E_B + \Delta F + F_0. \tag{S61}$$

$$F_{transition} = -E_A + F_0 + \Delta F^{\ddagger}_{unloop}. \tag{S62}$$

Here, F_0 is the reference state configurational free energy of the unlooped state. Hence, the activation energy of the forward path is $(F_{transition} - F_{looped}) = \Delta F^{\ddagger}_{loop}$. The activation energy of the reverse path is $(F_{transition} - F_{unlooped}) = \Delta F^{\ddagger}_{unloop}$. As a result, the on and off rate constants for operator B are given by

$$k^{\beta}_{on} = k^{\beta}_0 e^{-\beta \Delta F^{\ddagger}_{unloop}}. \tag{S63}$$

$$k^{\beta}_{off} = k^{\beta}_0 e^{-\beta \Delta F^{\ddagger}_{loop}} \propto e^{-\beta(\Delta F^{\ddagger}_{unloop} - \Delta F - E_B)} \propto e^{-\beta(\Delta F^{\ddagger}_{unloop} - \Delta F)}. \tag{S64}$$

Similarly, if we consider the transition between the state that only binding site B is bound and the looped state, we can obtain the rate constants for operator A as

$$k^{\alpha}_{on} = k^{\alpha}_0 e^{-\beta \Delta F^{\ddagger}_{unloop}}. \tag{S65}$$

$$k^{\alpha}_{off} = k^{\alpha}_0 e^{-\beta \Delta F^{\ddagger}_{loop}} \propto e^{-\beta(\Delta F^{\ddagger}_{unloop} - \Delta F - E_B)} \propto e^{-\beta(\Delta F^{\ddagger}_{unloop} - \Delta F)}. \tag{S66}$$

The above relationships automatically satisfy the detailed balance constraints given in Eq. S36 and S37 that $\frac{k^{\alpha}_{on}}{k^{\alpha}_{off}} \propto e^{-\beta \Delta F} \propto J_{loop}$ and $\frac{k^{\beta}_{on}}{k^{\beta}_{off}} \propto J_{loop}$.

Comparing the above on-rates in Eq. S63 and Eq. S65 with the relationship between unlooped lifetime and kinetic rates given in Eq. S55, we see that the experimentally measured unlooped lifetimes are governed by

$$< \tau_{unlooped} >= \frac{(1 + \frac{k^A_{off}}{[R]k^A_{on}})(1 + \frac{k^B_{off}}{[R]k^B_{on}})}{k^{\alpha}_{on}(\frac{k^A_{off}}{[R]k^A_{on}}) + k^{\beta}_{on}(\frac{k^B_{off}}{[R]k^B_{on}})} = \frac{(1 + \frac{k^A_{off}}{[R]k^A_{on}})(1 + \frac{k^B_{off}}{[R]k^B_{on}})}{k^{\alpha}_0 e^{-\beta \Delta F^{\ddagger}_{unloop}}(\frac{k^A_{off}}{[R]k^A_{on}}) + k^{\beta}_0 e^{-\beta \Delta F^{\ddagger}_{unloop}}(\frac{k^B_{off}}{[R]k^B_{on}})} \propto e^{\beta \Delta F^{\ddagger}_{unloop}}. \tag{S67}$$

On the other hand, comparing the above off-rates in Eq. S64 and Eq. S66 with the relation between looped lifetimes and kinetic rates given in Eq. S54, we see that the experimentally measured looped lifetimes are governed by

$$< \tau_{looped} >= \frac{1}{(k^{\alpha}_{off} + k^{\beta}_{off})} = \frac{1}{(k^{\alpha}_0 e^{-\beta(E_A + \Delta F^{\ddagger}_{unloop} - \Delta F)} + k^{\beta}_0 e^{-\beta(E_B + \Delta F^{\ddagger}_{unloop} - \Delta F)})} \propto e^{\beta(\Delta F^{\ddagger}_{unloop} - \Delta F)}. \tag{S68}$$

The lifetimes also satisfy the constraint from the looping probability given in Eq. S43 that $\frac{<\tau_{looped}>}{<\tau_{unlooped}>} \propto e^{-\beta \Delta F} \propto J_{loop}$.

S2.3.3 The transition state depends on the polymer construct.

For a polymer or a DNA-protein polymer system, the free energy of the closed or looped conformation involves an increase in elastic energy and a change in entropy due to constrained polymer fluctuations. The looped conformation and its elastic energy depend on the construct—specifically, the size, geometry and rigidities of the polymer system. The entropy change is also governed by the looped conformation and hence depends on the construct. As a result, the looping free energy and its structure are determined by the polymer system construct, even if the exact solution is not available for systems like protein-mediated DNA looping. On the other hand, despite the unknown structure of the transition state, we have some hints about what it should be. In computing the first passage time to polymer ring closure, the landscape of configurational free energy is usually calculated based on the polymer rigidities and size, and the system is modeled as diffusion in the free energy landscape (or effective potential) (38). The time scale to looping is thus given by the rate to cross a barrier whose height is determined by the polymer construct, applying some variations of the transition state theory (such as Kramer's theory). This scheme is identical to using transition state theory in our looping system, and the barrier height bears the same concept as what would be the transition state in our system. Hence, we argue that in our system the transition state free energy is also governed by the polymer construct. Since both the transition state free energy and the looping free energy are governed by the polymer construct, their values are related.

In other words, we argue that the transition state configurational free energy change $\Delta F^{\ddagger}_{unloop}$ is related to the looping free energy change ΔF, since they are both determined by the polymer construct. For a given construct whose ΔF is known, the value of $\Delta F^{\ddagger}_{unloop}$ is uniquely determined. There is a mapping from ΔF to $\Delta F^{\ddagger}_{unloop}$,

$$\Delta F^{\ddagger}_{unloop} = \Delta F^{\ddagger}_{unloop}(\Delta F). \tag{S69}$$

Then the unlooped and looped lifetimes given in Eq. S67 and S68 become

$$< \tau_{unlooped} > \propto e^{\beta \Delta F^{\ddagger}_{unloop}(\Delta F)}, \tag{S70}$$

and

$$< \tau_{looped} > \propto e^{\beta(\Delta F^{\ddagger}_{unloop}(\Delta F) - \Delta F)}. \tag{S71}$$

This means that the kinetic rates as well as the looped and unlooped lifetimes have to scale with $J_{loop} \propto e^{-\beta \Delta F}$. In particular, since $\Delta F \propto \frac{\ln J_{loop}}{-\beta}$,

$$< \tau_{unlooped} > \propto e^{\beta \Delta F^{\ddagger}_{unloop}(\Delta F)} \propto e^{\beta \Delta F^{\ddagger}_{unloop}[\frac{\ln J_{loop}}{-\beta}]} \tag{S72}$$

and

$$< \tau_{looped} > \propto e^{\beta(\Delta F^{\ddagger}_{unloop}(\Delta F) - \Delta F)} \propto e^{\beta(\Delta F^{\ddagger}_{unloop}(\Delta F)} \cdot e^{-\beta \Delta F} \propto e^{\beta(\Delta F^{\ddagger}_{unloop}[\frac{\ln J_{loop}}{-\beta}])} \cdot J_{loop}, \tag{S73}$$

showing that the lifetimes are functions of J_{loop} and hence the data collapse we observe in Figure 3a, b.

S2.3.4 Approximate power-law-like scaling.

Without knowing the exact form of $\Delta F^{\ddagger}_{unloop} = \Delta F^{\ddagger}_{unloop}(\Delta F)$, we can still estimate how $\Delta F^{\ddagger}_{unloop}$ and ΔF are related numerically. We ask what their relative numerical values are, quantified by the ratio n such that

$$\Delta F^{\ddagger}_{unloop}(\Delta F) = n \Delta F. \tag{S74}$$

Within a small perturbation of parameter space (in our case, the DNA constructs share a similar range of loop lengths and have similar helical repeats; their measured looping J-factors also fall within similar ranges), we can assume n is approximately constant over this range.

If we then insert Eq. S74 into the lifetimes given by Eq. S70 and Eq. S71, we get

$$< \tau_{unlooped} > \propto e^{\beta \Delta F^{\ddagger}_{unloop}(\Delta F)} = e^{\beta(n\Delta F)} \propto J_{loop}^{-n}, \tag{S75}$$

and

$$< \tau_{looped} > \propto e^{\beta(\Delta F^{\ddagger}_{unloop}(\Delta F) - \Delta F)} = e^{\beta(n-1)\Delta F} \propto J_{loop}^{-(n-1)}. \tag{S76}$$

Thus, we expect to see approximate power-law-like scaling of the lifetimes with respect to the looping J-factor, given by

$$\log\left(< \tau_{unlooped} >\right) = (-n)\log\left(J_{loop}\right) + constant, \tag{S77}$$

and

$$\log\left(< \tau_{looped} >\right) = (1-n)\log\left(J_{loop}\right) + constant. \tag{S78}$$

As noted above, protein-mediated DNA looping is complicated because of as-yet poorly-established boundary conditions. We propose this approximate power-law-like scaling observation as a way to probe looping transition state free energies, and that it may be useful in future simulation efforts. The development of the transition state theory has laid the groundwork to understand the dependence of both the loop formation and breakdown kinetics on the polymer properties encapsulated within the looping J-factor.

S2.4 Development of a molecular-level model for the transition state

S2.4.1 Defining the free energy landscape

In order to better incorporate the polymer elastic properties and understand how they uniquely contribute to the looped and unlooped lifetimes, we develop a molecular model that captures the competing effects of polymer deformation free energy and bonding energy. We approximate the DNA-Lac repressor complex (when one binding head of the repressor is bound at one of the binding sites on the DNA, leaving the other binding head of the repressor free and the other binding site empty) by an "effective polymer chain", which we describe with the wormlike chain model. For simplicity, hereafter we refer to the effective polymer chain as DNA. As for the bonding energy between the free repressor binding head and the empty DNA binding site, we consider a realistic energy profile with finite interaction length. The interplay between the bonding interaction length and the typical polymer deformation length scale determines the transition state. Since our experiments suggested a key role of the looping J-factor in determining the lifetimes of the looped and unlooped states, we wish to explore the properties of the polymer chain that fed into the J-factor and better understand how the lifetimes scale with these properties.

To begin, we consider the DNA as a wormlike chain that has a bending modulus $k_B T L_p$ (43). The persistence length, L_p, captures how long the polymer chain would prefer to extend in one direction. For double-stranded DNA, this is typically around 155 bp, or about 53 nm (44). The tangent vector as you move along the chain is ($\vec{u} = \frac{d\vec{r}}{ds}$). The bending energy for this continuous chain is given by

$$\beta E_{bend} = \frac{L_p}{2}\int_0^L ds \kappa(s)^2 \tag{S79}$$

and depends on the square of the local curvature $\kappa(s) = |\frac{d\vec{u}}{ds}|$. The local curvature is equivalent to the inverse of the radius of a circle that is tangent to the curve (*e.g.* a straight chain segment has zero curvature and a tangent circle with infinite radius). The local curvature captures the change in the tangent vector as you move along the chain, with a larger $\kappa(s)$ indicating that the the chain is more highly bent at location s.

We next calculate the resulting free energy of a polymer chain that has this elastic bending penalty, including both entropic effects and elastic deformation. To start, we find the Green function $G(r) to be$

$$G(r) = \int D\left[\vec{r}(s)\right] \exp\left(-\beta E_{bend}\right), \tag{S80}$$

which is the probability of finding the two ends or binding sites to be a distance r apart. The Green function is an average over all chain configurations, with each appropriately weighed by a Boltzmann term of the bending energy, with $\vec{r}(s)$ the position in space of the chain at point s. This is the partition function for the wormlike chain, and we have previously derived its exact result analytically (45). We calculate the Green function for a given chain length L and persistence length L_p using the methods outlined in Mehraeen et al. (2008) (46). The free energy $F_{conf}(r)$ of this chain is related to the Green function $G(r)$ as

$$F_{conf}(r) = -k_B T \log \left[r^2 G(r) \right]. \tag{S81}$$

The term in the logarithm represents the probability of finding the polymer with end-to-end distance between r and $r+dr$. At long end-to-end distances r, the fully elongated chain will have few conformations that it can access, carrying a high entropic penalty. When the two ends are close, there will also be a strong entropic penalty as well as an elastic penalty for bending the chain.

The DNA strand has an intrinsic twist, and since the Lac repressor binding interface is specific for a certain orientation of the DNA, the DNA strand will need to twist to bind the protein. The resistance to twisting is captured by an energetic penalty for twist deformation. The intervening DNA length, *i.e.* the length of the loop L, determines the undeformed orientation of the DNA helix at the operator, and proper alignment for binding incurs twist deformation upon rotating the DNA into its proper orientation. We define the twist angle θ to be the angle of rotation about the DNA axis at the unbound operator away from the ground-state untwisted angle (*i.e.* $\theta = 0$ is untwisted). We consider a simple model for the twist free energy, where

$$F_{twist}(\theta) = [k_B T L_t/(2L)]\theta^2, \tag{S82}$$

which is quadratic in the local twist deformation and evenly distributes the twist deformation over the length of the DNA between the operators. The twist persistence length L_t captures the resistance to twist deformation, and has typically been measured for DNA as 110 nm (47). This model neglects the geometric coupling between twist and writhe of the chain, which becomes more relevant at longer chains where out-of-plane conformations are not prohibited by the bending deformation energy (48). More detailed models incorporating twist require knowledge of the entry and exit angles of the DNA as it binds the Lac repressor (45). This model also neglects any entropic contributions to the orientation. These simplifications to the model for twist could result in differences between our measured parameter values for L_t and the canonical values.

The binding free energy, which drives the formation of the looped state is modeled as a potential well with depth ϵ_0 and an interaction length scale δ. The favorable binding energy increases as the operators are brought to closer proximity, with the length-scale δ determining at what distance the energy begins to be felt. Given the size of the Lac repressor arms as well as their ability to non-specifically bind the DNA the value of δ should be expected to be a few nanometers (14, 49, 50). The binding energy between the DNA operator and Lac repressor has previously been measured around 15-18 $k_B T$, so we would expect ϵ_0 to fall close to this range (51). The binding energy is also sensitive to the orientation of the binding sites. This effect can be introduced by calculating the distance of separation between two operators at the surface of DNA, which is illustrated in Fig. S5, given by

$$r_a(r, \theta) = \sqrt{(r-a)^2 + a^2 - 2(r-a)a\cos(\theta - \theta_{op})}. \tag{S83}$$

Here, as shown in Fig. S5, r is the end-to-end distance of the two DNA strands, θ is the twist angle at the unbound operator, θ_{op} is the preferred twist angle for binding, and a is the radius of the DNA helix (assumed to be $a = 1\,\text{nm}$) (52). Thus, when the orientation is away from the preferred binding angle, the unbound operator will be farther away from the Lac repressor due to the geometry of the DNA helix. The preferred twist angle $\theta_{op} = 2\pi(L/L_{turn}) + \theta_0$ gives the twist angle that orients the operator to face the Lac repressor binding site, where θ_0 defines the twist angle of the Lac repressor binding site. The

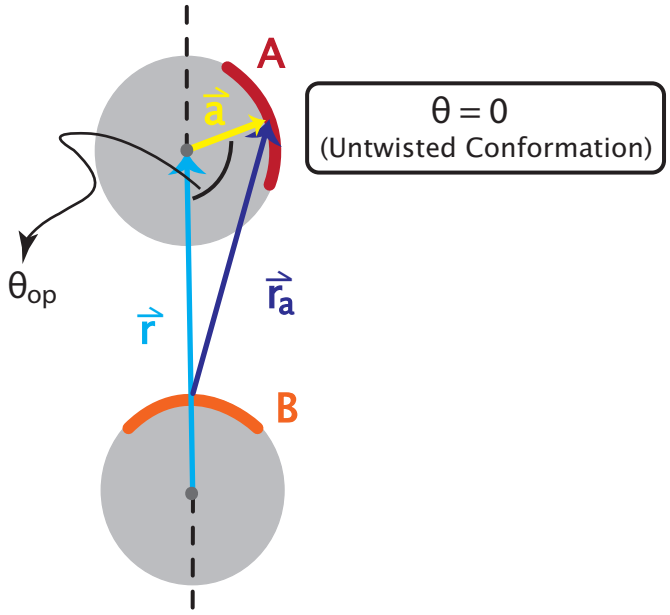

Figure S5: **Illustration of reaction coordinates.** Here we show the cross sectional view of the DNA strands (gray objects) with radius a and are separated by an end-to-end distance r. In order for the binding event to occur, the two operators A and B must be brought together by strand rotation to compensate θ_{op}. The rotational reaction coordinate about the DNA axis is θ, and in this illustration we show the $\theta = 0$ conformation for simplicity. Importantly, the binding energy $F_{bind}(r, \theta)$ has to do with the separation of operators at the DNA surface, hence is parametrized by r_a. The size of the repressor is neglected here, or, effectively, is absorbed into a.

binding free energy F_{bind} is given by

$$F_{bind}(r,\theta) = \begin{cases} \frac{-2\epsilon_0}{1+\exp\left[\frac{r_a(r,\theta)}{\delta}\right]}, & r > 2a, \\ \infty, & r \leq 2a, \end{cases} \tag{S84}$$

which includes a steric cutoff at $r = 2a$ to account for the overlap of DNA segments. This simple binding model aims to capture the basic interaction between the DNA operator and Lac repressor by introducing only the binding affinity ϵ_0 and the interaction length δ to capture the physical interaction. More detailed models of interaction could capture more molecular detail, but our goal is to give the simplest representation of binding without introducing additional parameters that do not have well-defined values.

The three thermodynamic contributions $F_{conf}(r)$, $F_{twist}(\theta)$, and $F_{bind}(r, \theta)$ combine to give the total free energy landscape $F_{total}(r, \theta)$, as shown in Fig. 4a of the main text, for $L = 101\,\text{bp}$ and parameters $\epsilon_0 = 23.5\,k_BT$, $\delta = 1.3\,\text{nm}$, $L_p = 48\,\text{nm}$, $L_t = 15\,\text{nm}$, and $\theta_0 = 0.003\,\pi$. We next find the minimum free energy path from the looped state in point X, over the transition state Y, to the unlooped state Z to reduce the two-dimensional free energy landscape down to a one-dimensional reaction along the end-to-end distance r. This minimum path is found by determining the value of θ that corresponds to the minimum of F_{total} for a given value of r. This is equivalent to use of the zero-temperature string method, which finds the minimum energy path by numerically moving along the surface along the gradient into valley which forms the minimum energy path. We used code adapted from E, Ren, and Vanden-Eijnden (2002) for this calculation (53). Using the minimum values of $\theta(r)$, we then plot each of the three energies, as well as the total, in Fig. 4b of the main text.

S2.4.2 Deriving the lifetimes and the looping J-factor

With our one-dimensional free energy landscape, $F_{total}(r)$, we can now proceed to calculate the experimentally determined quantities of the looping J-factor and the looped and unlooped lifetimes. The

J_{loop} calculated in the experiments corresponds to the free energy difference ΔF between the looped and unlooped states. This free energy difference includes the contributions to the polymer, but does not including the binding energy. To calculate J_{loop}, we first calculate F_{poly}^{loop}, which is

$$F_{poly}^{loop} = -\log Q_{loop} - \frac{\int_{2a}^{r_Y} dr F_{bind}(r) \exp\left[-\beta F_{total}(r)\right]}{Q_{loop}}, \tag{S85}$$

where the partition function $Q_{loop} = \int_{2a}^{r_Y} dr \exp\left[-\beta F_{total}(r)\right]$. The first term represents the total free energy of the looped state, defined from $r = 2a$ to $r = r_Y$ at the transition state Y, and the second term subtracts the binding energy $F_{bind}(r)$ over that region. We can similarly define F_{poly}^{unloop} for the unlooped state from r at the transition state to $r = L$ as

$$F_{poly}^{unloop} = -\log Q_{unloop} - \frac{\int_{r_Y}^{L} dr F_{bind}(r) \exp\left[-\beta F_{total}(r)\right]}{Q_{unloop}}, \tag{S86}$$

where here $Q_{unloop} = \int_{r_Y}^{L} dr \exp\left[-\beta F_{total}(r)\right]$. The looping J-factor can then be calculated from the polymer free energy difference,

$$J_{loop} = (1\,\mathrm{M}) \exp(-\beta \Delta F) = (1\,\mathrm{M}) \exp\left[-\beta (F_{poly}^{loop} - F_{poly}^{unloop})\right], \tag{S87}$$

where we have as in the experiments assumed a standard state of 1 M (1, 2).

We calculate the lifetimes of the looped and unlooped sate by use of the Fokker-Planck equation. The equation defines the motion of an object over a free energy landscape, and is given by

$$\left\{\frac{\partial}{\partial t} - \Gamma^R\right\} G^R(r', t|r, 0) = 0, \tag{S88}$$

where

$$\Gamma^R = D_{eff}\left(\frac{\partial^2}{\partial r^2} + \frac{\partial \beta F_{total}}{\partial r}\frac{\partial}{\partial r}\right). \tag{S89}$$

By solving Eq. S88 for our free energy landscape $F_{total}(r)$, we can calculate the flux of particles that cross the transition state in either direction and from that the time that is spent in either the looped or the unlooped state. We note that this is a more exact treatment to calculate the reaction rates given that we have a full free energy landscape defined at each point of the reaction coordinate r. From basic transition state theory, the looped and unlooped lifetimes will in general be dependent on the barrier heights given in Fig. 4b, and are proportional to $\exp(-\beta \Delta F_{loop}^{\ddagger})$ and $\exp(-\beta \Delta F_{unloop}^{\ddagger})$, respectively. Kramers theory improves on this approximation by defining the proportionality based on the curvatures at the minima and maximum of the free energy path, and is an approximation of the more complete Fokker-Planck treatment we use. We solve Eq. S88 numerically for a given set of model parameters. To begin, we define the mean passage time $T(r)$ as the time to go from end-to-end distance r to the barrier at the transition state, where $r = r_Y$. Following from Eq. S88, $T(r)$ is governed by

$$\Gamma^R T(r) = -1, \tag{S90}$$

with boundary conditions of $T(r = a) = 0$ and $\frac{\partial T}{\partial r}(r = 0) = 0$. Solving this equation for $T(r)$, and averaging over all end-to-end distances in the looped state (which goes from $r = 2a$ to $r = r_Y$), yields the mean looped lifetime

$$< \tau_{looped} >= D_{eff} \frac{\int_{2a}^{r_Y} dr \int_{r}^{r_Y} dr' \int_{2a}^{r'} dr'' \exp\left[-\beta F_{total}(r) + \beta F_{total}(r') - \beta F_{total}(r'')\right]}{Q_{loop}}. \tag{S91}$$

Similarly, we can find the mean unlooped lifetime

$$< \tau_{unlooped} >= D_{eff} \frac{\int_{r_Y}^{L} dr \int_{r_Y}^{r} dr' \int_{r'}^{L} dr'' \exp\left[-\beta F_{total}(r) + \beta F_{total}(r') - \beta F_{total}(r'')\right]}{Q_{unloop}}, \tag{S92}$$

where the unlooped state ranges from $r = r_Y$ to $r = L$. More details on this solution can be found in an upcoming manuscript that will expand upon the theory developed in this work.

To compare our results to the experiments, we must find model parameters for the elastic parameters L_p, L_t, which could vary by sequence, and the binding parameters ϵ_0, δ, and θ_0, which should be consistent across all sequences with the same operators. When looking at the J_{loop} data versus loop length, a peak occurs between 104 and 105 bp for all five sequences . At this peak, no twisting (*i.e.* $\theta = 0$) is needed to align the untwisted conformation angle ($2\pi L/L_{turn}$) to the preferred binding orientation θ_0. We chose a value of $\theta_0 = 0.003\,\pi$, which fit the peak value across all five sequences well and which corresponds to a peak occurring at a loop length of approximately 104.6 bp. Fixing this parameter, we calculated looping J-factors, looped and unlooped lifetimes for a range of the other four parameters. We then compared this output to the experimentally determined scaling law, calculating a sum of the squares deviation from this power law for each parameter realization of the model. Since a range of a parameter values could reproduce the basic scaling behavior, we chose the best fit to the power laws that fell within the experimental values of J_{loop}. Note that we had one free parameter D_{eff} that allowed us to rescale the lifetimes, and we determined $D_{eff} = 1.2 \times 10^{-5}\,\frac{\text{nm}^2}{\text{s}}$ to be the best fit to the data. Our selected values of $\epsilon_0 = 23.5\,k_BT$ and $\delta = 1.3\,\text{nm}$ provided a good fit to the data across all five sequences. Then, for each sequence, we chose the L_p and the L_t that were the best fit for those sequences given that $\epsilon_0 = 23.5\,k_BT$ and $\delta = 1.3\,\text{nm}$. This resulted in values of the persistence length L_p ranging from 48 to 51 nm and the twist persistence length L_t ranging from 10 to 70 nm. The model using the values for each sequence are shown compared to the experimental data in Fig. S6. We used the values from sequence TA in Fig. 4 in the main text.

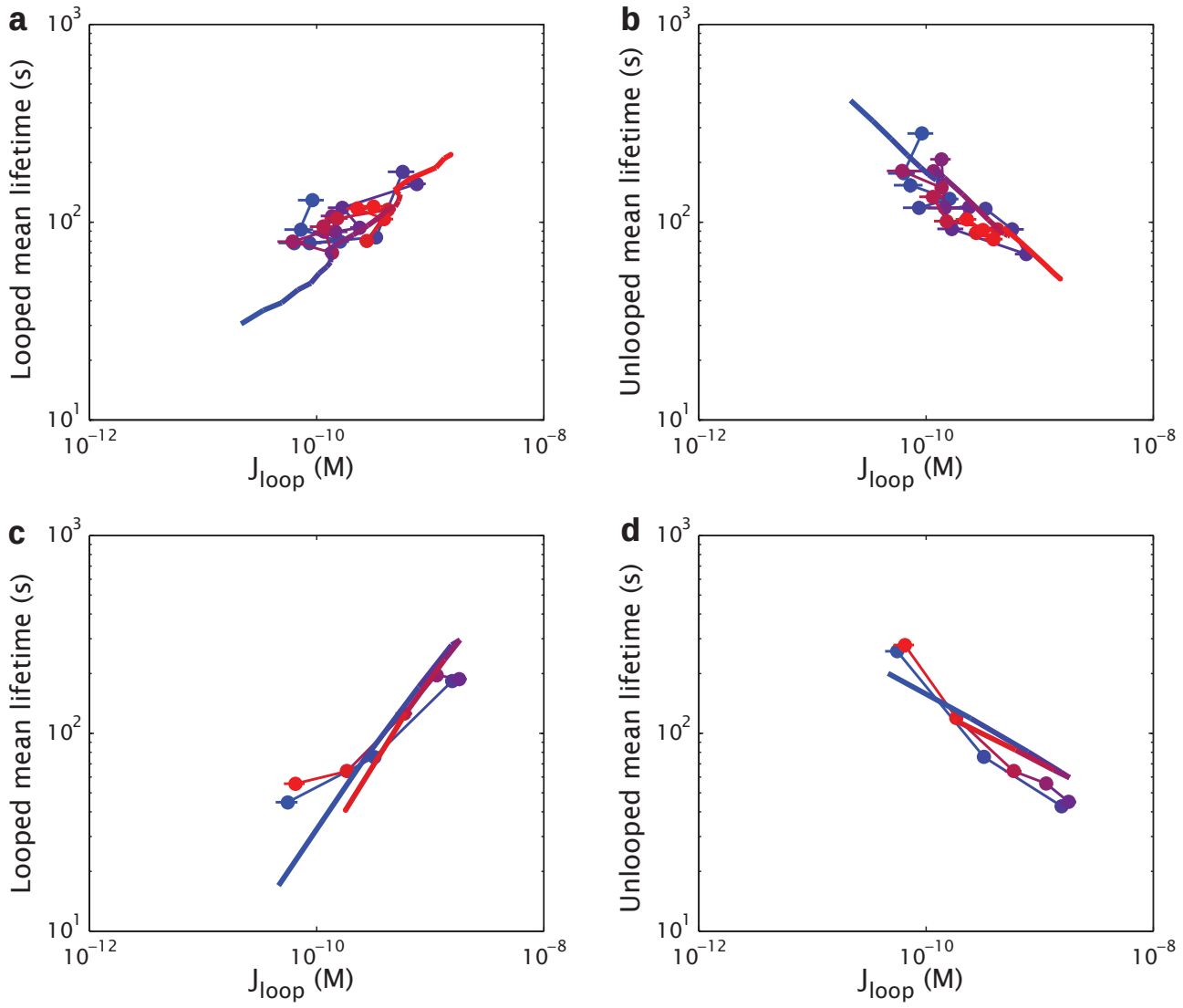

Figure S6: **WLC model for the energetics of DNA looping and its predictions.** The looped and unlooped lifetimes are shown for two of the five sequences. The parameters $\epsilon_0 = 23.5\,k_BT$, $\delta = 1.3\,\text{nm}$, and $\theta_0 = 0.003\,\pi\,\text{rad}$ are the same for all five sequences. The coloration varies from red (smallest) to blue (largest) based on the loop length. **a,b,** Looped and unlooped lifetime data (dots) and theory (lines) for sequence E8, with $L_p = 50\,\text{nm}$ and $L_t = 5\,\text{nm}$, and lengths varying from 89 to 115bp. **c,d,** Looped and unlooped lifetime data (dots) and theory (lines) for sequence dA, with $L_p = 46\,\text{nm}$ and $L_t = 50\,\text{nm}$, and lengths varying from 101 to 108bp.

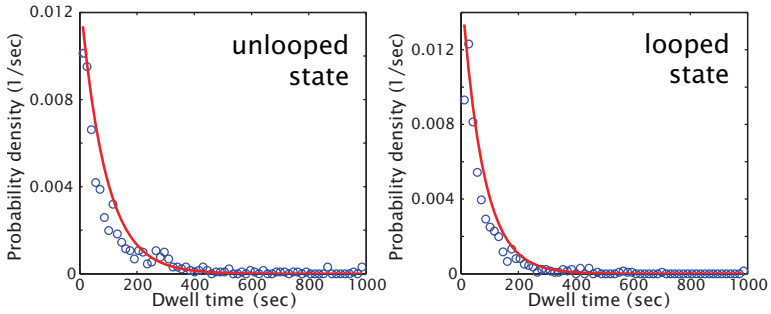

Figure S7: **Example lifetime histograms** for the construct Oid-E894-O1 in the presence of 100 pM repressor. Red curves are single exponential fits. This construct has only the middle looped state, whose lifetime distribution is shown in the right-hand panel. It is difficult to tell from these fits if a single exponential describes these distributions of lifetimes well, especially since we have found the results of the fits to vary significantly based on the size of the bins chosen. Here the bin size is 15 seconds. (Another way of avoiding binning is by plotting cumulative probability distributions, as in (22, 23), though we prefer the P-P plots described below for comparison to exponential distributions.)

S3 Additional Results

S3.1 Characteristics of the lifetime distributions.

In the main text we plot the means and standard errors of the lifetimes that we obtain for various data sets. Here we ask what the full distributions of these lifetimes look like, and in particular, whether they are exponentially distributed.

A state will have exponentially distributed lifetimes if it is composed of only one microstate, such that transitions out of the state are governed by a single rate constant. As shown in Fig. S2, we know there are 4 microstates that contribute to what we observe as the unlooped state (no repressor bound, a repressor bound at one operator, a repressor bound to the second operator, or both repressors bound by different operators—all of which should have comparable tether lengths). We would therefore expect that the lifetimes of the unlooped state would not be exponentially distributed; and indeed a kinetic analysis by Wong and coworkers on similar constructs to those used here (13), as well as one by Revalee and coworkers with longer loops and some intrinsically curved sequences (23), found the unlooped lifetime distributions to be best fit by a mixture of two exponentials. On the other hand, we might expect the middle and/or bottom looped states that we observe to be singly exponentially distributed, if they contain only one microstate, which is in fact what Wong and coworkers found (13). (Revalee and coworkers described only one looped state, which they found to be best fit by a biexponential distribution (23).)

A common method for determining whether lifetime distributions are exponentially distributed is to make histograms of the lifetimes, and fit exponentials to them (*e.g.*, (13, 17, 22)). An example of such histograms with a single-exponential fit is shown in Fig. S7. However, we have found the fidelity of this method to be subject to a significant amount of variability depending on the size of the bins chosen for the histogram, so instead here we use P–P ("percent–percent") plots to compare the empirical cumulative distribution functions (CDF) of the measured lifetimes we obtain to the CDF of an exponential distribution fit according to maximum likelihood.[3]

As shown in Fig. S8, we find most of the states we observe are not exponentially distributed. The only lifetimes that we find to be exponentially distributed are those of the unlooped state at or above 500 pM repressor concentration. As discussed in (1), at high repressor concentrations (that is, above the concentration at which looping is maximal, which includes 500 pM) we expect the unlooped state to be dominated by the microstate in which both operators are bound by separate repressors; the construct shown in Fig. S8b has the added advantage that its two flanking operators are the same, which collapses

[3]We are grateful to Matthew Johnson for the suggestion to use P–P plots and for the code to do the analysis, which can be freely downloaded from https://gist.github.com/mattjj/2356182 and https://gist.github.com/mattjj/5604903#file-qq-py.

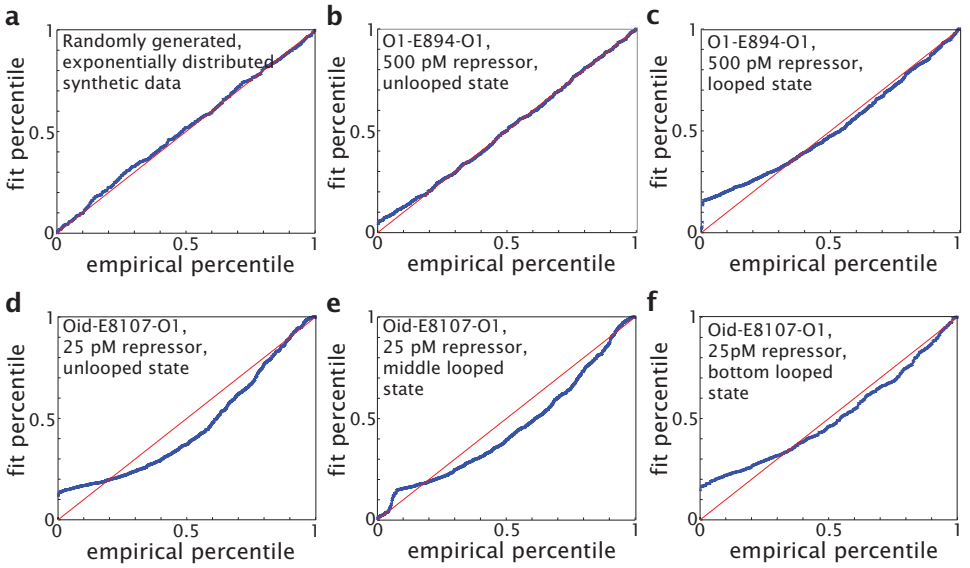

Figure S8: **P-P plots of the lifetimes that we obtain demonstrate that only one of our lifetime distributions is singly-exponentially distributed. a,** A P-P plot with randomly generated, exponentially distributed synthetic "data," with the same number of points as our lifetime distributions. When the empirical percentiles match the percentiles of the fit distribution, the plotted points (blue circles) will lie on the $y = x$ line (shown in red); the deviation of the points from the $y = x$ line measures the deviation of the empirical (measured) percentiles from the fit percentiles (and hence the deviation of the data from the fit model, in this case, an exponential). **b,** A P-P plot for the lifetimes obtained for the O1-E894-O1 construct's unlooped state at 500 pM repressor, compared to the cdf of a single exponential. In this case we conclude that a single exponential describes the experimental distribution well. **c,** A P-P plot for the same construct as in **b** but for the middle state. A single exponential does not describe these data well. **d-f,** P-P plots for a 107 bp loop of the E8 sequence flanked by the O_{id} and O_1 operators, at 25 pm repressor, a concentration at which both looped states are prevalent. None of these states is well-described by a single exponential, indicating that they most likely contain multiple microstates. The same holds for the other sequences, loop lengths, flanking operators and repressor concentrations lower than 500 pM that we have examined in this work. Note the common feature of blue points lying above the $y = x$ line at small percentiles, even in **b**, indicating that the measured lifetimes had too few counts at small values for the distribution to be well fit by an exponential; we suspect this feature is due at least in part to our limited temporal resolution which does not allow us to measure lifetimes shorter than 11 seconds.

the four possible unlooped state microstates into 3 microstates (the singly-bound-operator states being identical in this case). The majority of our constructs, under the majority of repressor concentrations, do not show singly-exponentially distributed lifetime distributions for either their looped or unlooped states, indicating that all are composed of multiple microstates. We have in fact recently shown using a more sophisticated kinetic analysis of a subset of the data discussed in this work that the two looped states we observe are indeed composed of multiple microstates (30), as has been long supposed to be the case (11, 12, 14, 54), and which again is consistent with the characteristics of the lifetime distributions we obtain here.

S3.2 Comparing looping rate constants for a loop flanked by identical operators to literature values.

For exponentially-distributed lifetimes, which characterize states whose exit rates are governed by a single rate constant, the rate constant for transitioning out of that state is simply the inverse of the mean lifetime of the state (see Sec. S2.1.4 above). As discussed in the previous section, we obtain exponentially distributed lifetimes only for the unlooped state at or above 500 pM. But at least for the unlooped state of those constructs that we have measured at high repressor concentration, we can compare the rate constants that we obtain to those recently reported by Wong and coworkers and Rutkauskas and coworkers on similar constructs, at the same salt concentrations that we use, and analyzed using half-amplitude threholding as we have done here (13, 28).

Wong and coworkers found their 133 bp and 138 bp loops, flanked by two O_{id} operators, to have unlooping rates (k^{α}_{off} in the language of Fig. S2, where in this case operators A and B are identical so $k^{\alpha}_{off} = k^{\beta}_{off}$) of 0.003 to 0.006 per second, and looping rates (k^{α}_{on}) of 0.005 to 0.03 per second, in the presence of 5.4 nM repressor. Rutkauskas and coworkers used a 285-bp loop flanked by two O_1 operators, and found unlooping rates from 0.023 to 0.046 per second. (As an aside, we note that the off-rate for O_1 in the absence of loop formation is 0.0047 per second as measured using nitrocellulose filter binding in 200 mM KCl (55), the same conditions as here and in (13, 28)).

If we assume exponentially-distributed lifetimes for our O1-E894-O1 construct at 500 pM repressor (shown in Fig. S8b and c above), we find a looping rate of roughly 0.005 per second, which is on the lower end of the range of values Wong and coworkers found with the stronger O_{id} operator. If we were to assume that the looped state is likewise also governed by only one rate constant (which is however unlikely, given the results of Sec. S3.1 above), we would calculate $k^{\alpha}_{off} \approx 0.02$ s^{-1}, which is faster than that of Wong and coworkers (which makes sense, given our weaker operator), and in good agreement with the values obtained by Rutkauskas and coworkers. Thus we are confident that our application of the half-amplitude thresholding method gives us reasonable values for approximate rate constants.

S3.3 Approximate power-law-like scaling of lifetimes with J-factor as a function of flanking operators, and for the two states separately.

In the main text we show that both unlooped and looped state lifetimes have a power-law-like relationship to looping J-factors. In Fig. S9a and b we show that this relationship holds when one of the flanking operators is changed (and the LacUV5 promoter sequence is added to the loop, because these sequences were originally designed for complementary *in vivo* and *in vitro* studies, with the promoter and the choice of operators being necessary for the *in vivo* work) (1, 2). In Fig. S9a and b as well as in Fig. 3 in the main text, the data are fit to a generic power law, as described in Sec. S1.4, with fit parameters given in Table S1. In Fig. S9c and d, we show the same data but fit to Eqs. S75 amd S76 in Sec. S2.3.4; these fit parameters are given in the bottom half of Table S1 (called "U/L, global").

Finally, in Fig. S10 we show the result of the lifetime analysis in which the middle and bottom looped states are thresholded separately (see Sec. S1.2), for both sets of flanking operators, again fit to generic power laws. Note that here we plot the middle looped state lifetimes against the looping J-factors of the

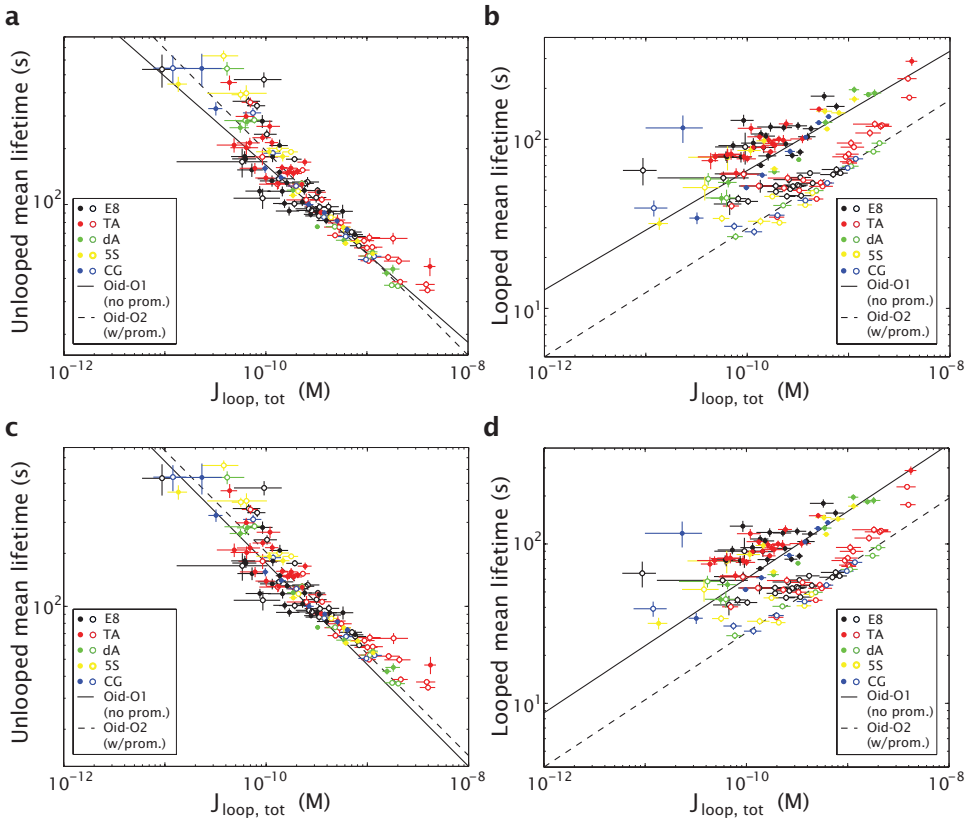

Figure S9: **Additional lifetimes data as a function of J-factor and flanking operators.** Unlooped state (**a, c**) and looped state (**b, d**) lifetimes as a function of J-factor and flanking operators. Closed circles are the same as those shown in the main text, and represent constructs flanked by the O_{id} and O_1 operators; open circles are constructs in which 36 bp of the loop have been replaced by the LacUV5 promoter sequence, and the flanking operators are O_{id} and O_2, O_2 being about five times weaker than O_1. Lines in **a** and **b** represent fits to generic power laws, with fit parameters given in the top five rows of the three lefthand columns of Table S1; lines in **c** and **d** represent a global fit of all four data sets (looped and unlooped states with two combinations of operators) to Eqs. S75 amd S76 in Sec. S2.3.4, with fit parameters given in the bottom half of Table S1.

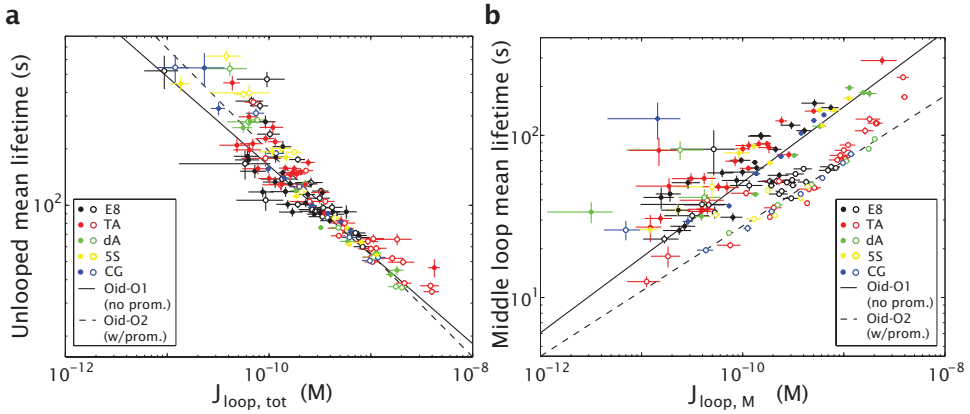

Figure S10: **Lifetimes vs. J-factors as a function of flanking operators**, when the two looped states are considered separately. Here the lifetimes for the middle state are plotted versus the looping J-factors for the middle state only, instead of the total looping J-factors used in the other plots here and in the main text. Lines represent fits to generic power laws, with fit parameters given in the top five rows of the three righthand columns in Table. S1.

middle state, rather than the total looping J-factor of both looped states combined. As noted above, for most constructs, especially the ones flanked by O_{id} and O_2 (and containing the promoter), the bottom state has such a low probability that $J_{loop,M}$ and $J_{loop,tot}$ are comparable. Note also that whether or not trajectories are thresholded according to unlooped-looped or unlooped-middle-bottom does not change the lifetimes of the unlooped state, as we would expect.

U/L	**a (sec/M)**	**b (unitless)**	**U/M/B**	**a (sec/M)**	**b (unitless)**
$\mathbf{U}_{Oid-O1}$	$28(\pm6)\times10^{-4}$	-0.48 ± 0.03	$\mathbf{U}_{Oid-O1}$	$29(\pm7)\times10^{-4}$	-0.48 ± 0.03
$\mathbf{U}_{Oid-O2}$	$6(\pm2)\times10^{-4}$	-0.55 ± 0.02	$\mathbf{U}_{Oid-O2}$	$6(\pm2)\times10^{-4}$	-0.55 ± 0.02
$\mathbf{L}_{Oid-O1}$	$2.2(\pm0.4)\times10^{5}$	0.35 ± 0.02	$\mathbf{M}_{Oid-O1}$	$2.3(\pm0.3)\times10^{6}$	0.5 ± 0.1
$\mathbf{L}_{Oid-O2}$	$1.9(\pm0.4)\times10^{5}$	0.385 ± 0.02	$\mathbf{M}_{Oid-O2}$	$2.9(\pm0.7)\times10^{5}$	0.4 ± 0.1
U/L, global	$\mathbf{C}_{U,Oid-O1}$ **(sec/M)**	$\mathbf{C}_{U,Oid-O2}$ **(sec/M)**	$\mathbf{C}_{L,Oid-O1}$ **(sec/M)**	$\mathbf{C}_{L,Oid-O2}$ **(sec/M)**	m **(unitless)**
	$2.9(\pm0.2)\times10^{-4}$	$3.4(\pm0.2)\times10^{-4}$	$1.00(\pm0.08)\times10^{6}$	$4.6(\pm0.4)\times10^{5}$	-0.422 ± 0.009

Table S1: Fit parameters for lifetimes as a function of J-factor. Two kinds of fits were performed on each of four data sets (unlooped vs. looped state, and O_{id}-O_1 vs O_{id}-O_2 as flanking operators): individual fits of each data set separately to a generic power law of the form $\langle\tau\rangle = a\times J_{loop}^{b}$, the parameters for which are given in the top left half of the table ("U/L"); or a global fit to all four data sets simultaneously to Eqs. S75 and S76 in Sec. S2.3.4, in which the m parameters was forced to be the same for all four data sets, but with the proportionality constants (here called C) allowed to be different for the looped vs. unlooped states and the two pairs of flanking operators. Fit parameters for this global fit are given in the bottom half of the table ("U/L, global"). In addition, we also performed fits to generic power laws for the analysis in which the middle and bottom looped states were thresholded separately, with parameters given in the top right half of the table ("U/M/B"). For most constructs the occurrence of the bottom state is too rare to allow a similar analysis on the bottom state.

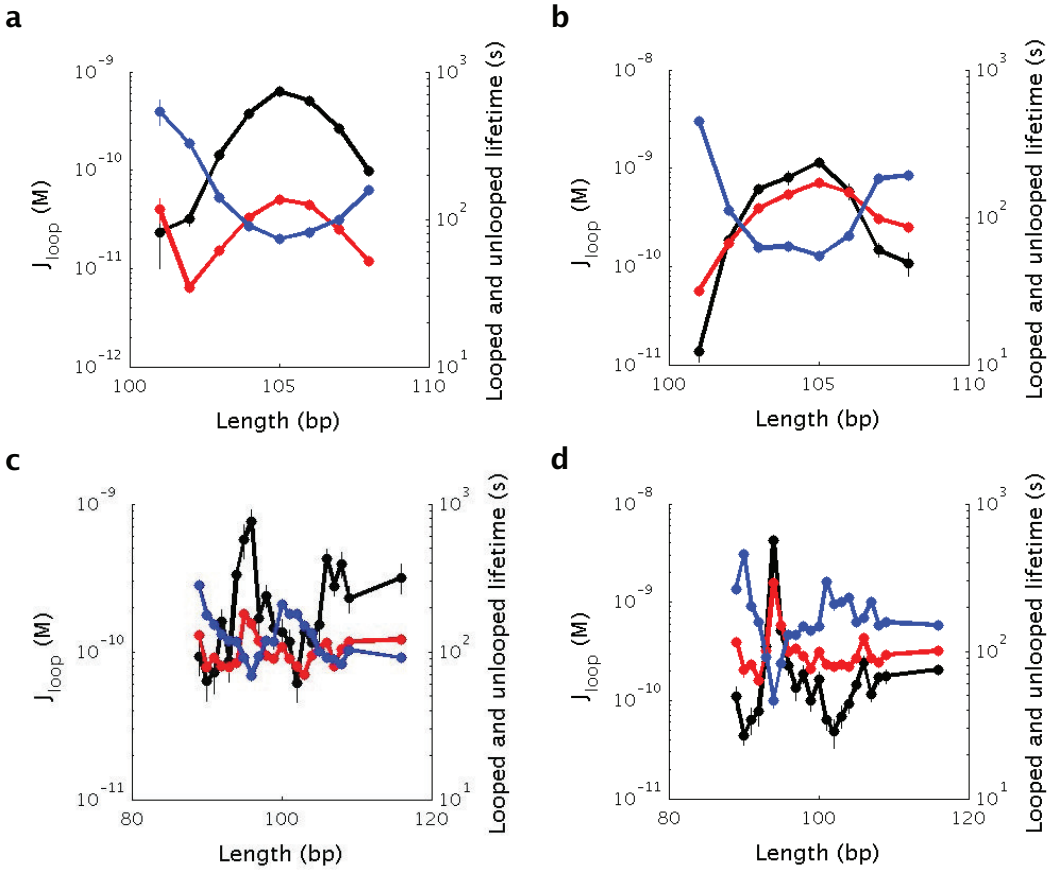

Figure S11: Unlooped (blue) lifetimes, looped (red) lifetimes, and looping J-factors (black) plotted as a function of loop length, for the DNA sequences **a,** CG, **b,** 5S, **c,** E8, **d,** TA.

References

[1] Johnson, S., Lindén, M. & Phillips, R. Sequence dependence of transcription factor-mediated DNA looping. *Nucleic Acids Res* **40**, 7728–7738 (2012).

[2] Johnson, S., Chen, Y.-J. & Phillips, R. Poly(dA:dT)-rich DNAs are highly flexible in the context of DNA looping. *PLoS ONE* **8**, e75799 (2013).

[3] Cloutier, T. E. & Widom, J. Spontaneous sharp bending of double-stranded DNA. *Molec Cell* **14**, 355–362 (2004).

[4] Cloutier, T. E. & Widom, J. DNA twisting flexibility and the formation of sharply looped protein-DNA complexes. *Proc Natl Acad Sci USA* **102**, 3645–3650 (2005).

[5] Lowary, P. T. & Widom, J. New DNA sequence rules for high affinity binding to histone octamer and sequence-directed nucleosome positioning. *J Mol Biol* **276**, 19–42 (1998).

[6] Simpson, R. T. & Stafford, D. W. Structural features of a phased nucleosome core particle. *Proc Natl Acad Sci USA* **80**, 51–55 (1983).

[7] Yuan, G.-C. *et al.* Genome-scale identification of nucleosome positions in *S. cerevisiae*. *Science* **309**, 627–630 (2005).

[8] Field, Y. *et al.* Distinct modes of regulation by chromatin encoded through nucleosome positioning signals. *PLoS Comput Biol* **4**, e1000216 (2008).

[9] Peters, J. P. & Maher 3rd, L. J. DNA curvature and flexibility *in vitro* and *in vivo*. *Quart Rev Biophys* **43**, 22–63 (2010).

[10] Haeusler, A. R. *et al.* FRET studies of a landscape of Lac repressor-mediated DNA loops. *Nucleic Acids Res* (2012).

[11] Swigon, D., Coleman, B. D. & Olson, W. K. Modeling the Lac repressor-operator assembly: the influence of DNA looping on Lac repressor conformation. *Proc Natl Acad Sci USA* **103**, 9879–9884 (2006).

[12] Zhang, Y., McEwen, A. E., Crothers, D. M., Levene, S. D. & Fraser, P. Analysis of *in vivo* LacR-mediated gene repression based on the mechanics of DNA looping. *PLoS One* **1**, e136 (2006).

[13] Wong, O. K., Guthold, M., Erie, D. A. & Gelles, J. Interconvertible Lac repressor-DNA loops revealed by single-molecule experiments. *PLoS Biol* **6**, e232 (2008).

[14] Czapla, L., Grosner, M., Swigon, D. & Olson, W. K. Interplay of Protein and DNA structure revealed in simulations of the *lac operon*. *PLOS ONE* **8**, e56548 (2013).

[15] Schafer, D. A., Gelles, J., Sheetz, M. P. & Landick, R. Transcription by single molecules of RNA polymerase observed by light microscopy. *Nature* **352**, 444–448 (1991).

[16] Yin, H., Landick, R. & Gelles, J. Tethered particle motion method for studying transcript elongation by a single RNA polymerase molecule. *Biophys J* **67**, 2468–2478 (1994).

[17] Finzi, L. & Gelles, J. Measurement of Lactose repressor-mediated loop formation and breakdown in single DNA molecules. *Science* **267**, 378–380 (1995).

[18] Nelson, P. C. *et al.* Tethered particle motion as a diagnostic of DNA tether length. *J Phys Chem B* **110**, 17260–17267 (2006).

[19] Colquhoun, D. & Sakmann, B. Fluctuations in the microsecond time range of the current through single acetylcholine receptor ion channels. *Nature* **294**, 464–466 (1981).

[20] Vanzi, F., Broggio, C., Sacconi, L. & Pavone, F. S. Lac repressor hinge flexibility and DNA looping: single molecule kinetics by tethered particle motion. *Nucleic Acids Res* **34**, 3409–3420 (2006).

[21] Laurens, N. *et al.* Dissecting protein-induced DNA looping dynamics in real time. *Nucleic Acids Res* **37**, 5454–5464 (2009).

[22] Laurens, N. *et al.* DNA looping by FokI: the impact of twisting and bending rigidity on protein-induced looping dynamics. *Nucleic Acids Res* **40**, 4988–4997 (2012).

[23] Revalee, J., Blab, G., Wilson, H., Kahn, J. & Meiners, J.-C. Tethered particle motion reveals that LacI·DNA loops coexist with a competitor-resistant but apparently unlooped conformation. *Biophys J* **106**, 705–715 (2014).

[24] Han, L. *et al.* Concentration and length dependence of DNA looping in transcriptional regulation. *PLoS One* **4**, e5621 (2009).

[25] Edelman, L. M., Cheong, R. & Kahn, J. D. Fluorescence resonance energy transfer over 130 basepairs in hyperstable Lac repressor-DNA loops. *Biophys J* **84**, 1131–1145 (2003).

[26] Morgan, M. A., Okamoto, K., Kahn, J. & English, D. S. Single-molecule spectroscopic determination of *lac* repressor-DNA loop conformation. *Biophys J* **89**, 2588–2596 (2005).

[27] Normanno, D., Vanzi, F. & Pavone, F. S. Single-molecule manipulation reveals supercoiling-dependent modulation of *lac* repressor-mediated DNA looping. *Nucleic Acids Res* **36**, 2505–2513 (2008).

[28] Rutkauskas, D., Zhan, H., Matthews, K. S., Pavone, F. S. & Vanzi, F. Tetramer opening in LacI-mediated DNA looping. *Proc Natl Acad Sci USA* **106**, 16627–16632 (2009).

[29] Mehta, R. A. & Kahn, J. D. Designed hyperstable Lac repressor·DNA loop topologies suggest alternative loop geometries. *J Mol Biol* **294**, 67–77 (1999).

[30] Johnson, S., van de Meent, J.-W., Phillips, R., Wiggins, C. & Lindén, M. Multiple LacI-mediated loops revealed by Bayesian statistics and tethered particle motion. *under review at Nucleic Acids Res* (2014).

[31] Bronson, J. E., Fei, J., Hofman, J. M., Jr., R. L. G. & Wiggins, C. H. Learning rates and states from biophysical time series: A Bayesian approach to model selection and Single-Molecule FRET data. *Biophys. J.* **97**, 3196–3205 (2009).

[32] Persson, F., Lindén, M., Unoson, C. & Elf, J. Extracting intracellular diffusive states and transition rates from single-molecule tracking data. *Nature Methods* **10**, 265–269 (2013).

[33] Colquhoun, D. & Sigworth, F. J. Fitting and statistical analysis of single-channel records. In Sakmann, B. & Neher, E. (eds.) *Single Channel Recording*, 191–263 (Plenum Press, 1983).

[34] Manzo, C. & Finzi, L. Quantitative analysis of DNA-looping kinetics from Tethered Particle Motion experiments. *Methods Enzymol* **475**, 199–220 (2010).

[35] Hippel, P., A., R., Gross, C. & Wang, A. Non-specific DNA binding of genome regulating proteins as a biological control mechanism: 1. The lac operon: equilibrium aspects. *Proc. Natl. Acad. Sci. USA* **71**, 4808–4812 (1974).

[36] Manzo, C., Zurla, C., Dunlap, D. & Finzi, L. The effect of nonspecific binding of lambda repressor on DNA looping dynamics. *Biophys J* **103**, 1753–1761 (2012).

[37] Law, S., Bellomy, G., Schlax, P. & Record, M. *In vivo* thermodynamic analysis of repression with and without looping in lac constructs. Estimates of free and local lac repressor concentrations and of physical properties of a region of supercoiled plasmid DNA *in vivo*. *J. Mol. Bio.* **230**, 161–173 (1993).

[38] Jun, S., Bechhoefer, J. & Ha, B. Y. Diffusion-limited loop formation of semiflexible polymers: Kramers theory and the intertwined time scales of chain relaxation and closing. *Europhys Lett* **64**, 420426 (2003).

[39] Hyeon, C. & Thirumalai, D. Kinetics of interior loop formation in semiflexible chains. *J Chem Phys* **124**, 104905 (2006).

[40] Toan, N., Morrison, G., Hyeon, C. & Thirumalai, D. Kinetics of loop formation in polymer chains. *J Phys Chem B* **112**, 6094–6106 (2008).

[41] Van Valen, D., Haataja, M. & Phillips, R. Biochemistry on a Leash: The Roles of Tether Length and Geometry in Signal Integration Proteins. *Biophys J* **96**, 12751292 (2009).

[42] Phillips, R., Kondev, J., Theriot, J., Garcia, H. G. & Orme, N. Physical biology of the cell, second edition, Garland Science, 2012 (2012).

[43] Saitô, N., Takahashi, K. & Yunoki, Y. The statistical mechanical theory of stiff chains. *Journal of the Physical Society of Japan* **22**, 219–226 (1967).

[44] Smith, S. B., Finzi, L. & Bustamante, C. Direct mechanical measurements of the elasticity of single dna molecules by using magnetic beads. *Science* **258**, 1122–1126 (1992).

[45] Spakowitz, A. Wormlike chain statistics with twist and fixed ends. *Europhys Lett* **73**, 684–690 (2006).

[46] Mehraeen, S., Sudhanshu, B., Koslover, E. F. & Spakowitz, A. J. End-to-end distribution for a wormlike chain in arbitrary dimensions. *Physical Review E* **77**, 061803 (2008).

[47] Bryant, Z. *et al.* Structural transitions and elasticity from torque measurements on dna. *Nature* **424**, 338–341 (2003).

[48] Sayar, M., Avşaroğlu, B. & Kabakçıoğlu, A. Twist-writhe partitioning in a coarse-grained dna minicircle model. *Physical Review E* **81**, 041916 (2010).

[49] Lewis, M. *et al.* Crystal structure of the lactose operon repressor and its complexes with DNA and inducer. *Science* **271**, 1247–1254 (1996).

[50] Kalodimos, C. G. *et al.* Structure and flexibility adaptation in nonspecific and specific protein-dna complexes. *Science* **305**, 386–389 (2004).

[51] Garcia, H. G. & Phillips, R. Quantitative dissection of the simple repression input–output function. *Proceedings of the National Academy of Sciences* **108**, 12173–12178 (2011).

[52] Sinden, R. R. *DNA structure and function* (Gulf Professional Publishing, 1994).

[53] Weinan, E., Ren, W. & Vanden-Eijnden, E. String method for the study of rare events. *Physical Review B* **66**, 052301 (2002).

[54] Towles, K. B., Beausang, J. F., Garcia, H. G., Phillips, R. & Nelson, P. C. First-principles calculation of DNA looping in tethered particle experiments. *Phys Biol* **6**, 025001 (2009).

[55] Winter, R., Berg, O. & von Hippel, P. Diffusion-driven mechanisms of protein translocation on nucleic acids. 3. The *Escherichia coli* lac repressor-operator interaction: kinetic measurements and conclusions. *Biochemistry* **20**, 6961–6977 (1981).